The relationship between CM and CO chondrites: Insights from combined analyses of titanium, chromium, and oxygen isotopes in CM, CO, and ungrouped chondrites

Journal Item

Available online at www.sciencedirect.com

ScienceDirect

Geochimica et Cosmochimica Acta 301 (2021) 70–90

Geochimica et Cosmochimica Acta

www.elsevier.com/locate/gca

The relationship between CM and CO chondrites: Insights from combined analyses of titanium, chromium, and oxygen isotopes in CM, CO, and ungrouped chondrites

Zachary A. Torrano [a,*], Devin L. Schrader [a,b], Jemma Davidson [a,b] Richard C. Greenwood [c], Daniel R. Dunlap [a,1], Meenakshi Wadhwa [a]

[a] School of Earth and Space Exploration, Arizona State University, Tempe, AZ 85287, USA
[b] Center for Meteorite Studies, Arizona State University, Tempe, AZ 85287, USA
[c] Planetary and Space Sciences, School of Physical Sciences, The Open University, Milton Keynes MK7 6AA, United Kingdom

Received 6 December 2020; accepted in revised form 2 March 2021; Available online 10 March 2021

Abstract

A close relationship between CM and CO chondrites has been suggested by previous petrologic and isotopic studies, leading to the suggestion that they may originate from similar precursor materials or even a common parent body. In this study, we evaluate the genetic relationship between CM and CO chondrites using Ti, Cr, and O isotopes. We first provide additional constraints on the ranges of ε^{50}Ti and ε^{54}Cr values of bulk CM and CO chondrites by reporting the isotopic compositions of CM2 chondrites Murchison, Murray, and Aguas Zarcas and the CO3.8 chondrite Isna. We then report the ε^{50}Ti and ε^{54}Cr values for several ungrouped and anomalous carbonaceous chondrites that have been previously reported to exhibit similarities to the CM and/or CO chondrite groups, including Elephant Moraine (EET) 83226, EET 83355, Grosvenor Mountains (GRO) 95566, MacAlpine Hills (MAC) 87300, MAC 87301, MAC 88107, and Northwest Africa (NWA) 5958, and the O-isotope compositions of a subset of these samples. We additionally report the Ti, Cr, and O isotopic compositions of additional ungrouped chondrites LaPaz Ice Field (LAP) 04757, LAP 04773, Lewis Cliff (LEW) 85332, and Coolidge to assess their potential relationships with known carbonaceous and ordinary chondrite groups. LAP 04757 and LAP 04773 exhibit isotopic compositions indicating they are low-FeO ordinary chondrites. The isotopic compositions of Murchison, Murray, Aguas Zarcas, and Isna extend the compositional ranges defined by the CM and CO chondrites in ε^{50}Ti versus ε^{54}Cr space. The majority of the ungrouped carbonaceous chondrites with documented similarities to the CM and/or CO chondrites plot outside the CM and CO group fields in plots of ε^{50}Ti versus ε^{54}Cr, Δ^{17}O versus ε^{50}Ti, and Δ^{17}O versus ε^{54}Cr. Therefore, based on differences in their Ti, Cr, and O isotopic compositions, we conclude that the CM, CO, and ungrouped carbonaceous chondrites likely represent samples of multiple distinct parent bodies. We also infer that these parent bodies formed from precursor materials that shared similar isotopic compositions, which may indicate formation in regions of the protoplanetary disk that were in close proximity to each other.

Keywords: Chromium; Titanium; Oxygen; Isotopes; Carbonaceous chondrites; CM chondrites; CO chondrites

1. INTRODUCTION

The isotopic compositions of meteorites provide forensic clues to the source regions of their parent bodies and enable evaluation of potential genetic relationships between

* Corresponding author at: Earth and Planets Laboratory, Carnegie Institution for Science, Washington, DC 20015, USA.
E-mail address: ztorrano@carnegiescience.edu (Z.A. Torrano).
[1] Present address: Lunar and Planetary Institute, Houston, TX 77058, USA

https://doi.org/10.1016/j.gca.2021.03.004
0016-7037/

samples and known meteorite groups. Many previous studies have used O-isotope compositions of meteorites to identify common nebular source reservoirs and establish genetic relationships (e.g., Clayton, 1993; Clayton and Mayeda, 1996, 1999). More recently, Cr and Ti isotopes (often in combination with O isotopes) have also been found to be useful isotopic tracers of distinct Solar System reservoirs (e.g., Warren, 2011; Sanborn et al., 2019). A fundamental dichotomy has been identified between "non-carbonaceous chondritic" (NC) and "carbonaceous chondritic" (CC) Solar System materials in a variety of isotope systems (Fig. 1; e.g., Kruijer et al., 2020 and references therein). As such, these materials are thought to have formed in distinct isotopic reservoirs in the inner (NC) and outer (CC) Solar System (Warren, 2011). These distinct reservoirs are thought to have coexisted from ~1 Ma to 3–4 Ma after Solar System formation, likely remaining separated because of the formation and growth of Jupiter (Kruijer et al., 2017) or a pressure maximum in the disk near Jupiter's location (Brasser and Mojzsis, 2020). Therefore, combined analyses of the Ti, Cr, and O isotopic compositions of meteorites can serve as powerful tracers for assessing potential genetic relationships between meteorite parent bodies and can shed light on mixing processes and evolution in the protoplanetary disk.

The Mighei-like (CM) and Ornans-like (CO) carbonaceous chondrites are collectively considered to be the CM–CO clan (Weisberg et al., 2006) on the basis of mineralogical and chemical similarities. The study of CM chondrites is especially timely because spectral properties and albedo measurements of CM chondrites are similar to those reported for the B-type asteroid Bennu and the C-type asteroid Ryugu by the NASA OSIRIS-REx and JAXA Hayabusa2 sample

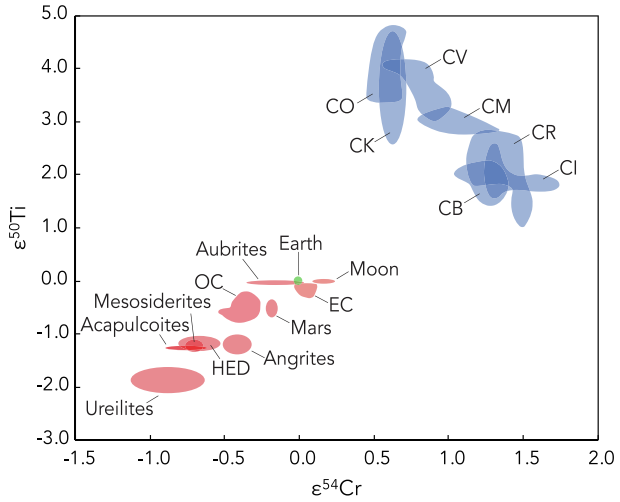

Fig. 1. Plot of ε^{50}Ti versus ε^{54}Cr for CC (blue) and NC (red) meteorites, with Earth shown in green. Data fields are drawn based on data from Shukolyukov and Lugmair (2006), Trinquier et al. (2007, 2009), Qin et al. (2010), Yamakawa et al. (2010); Yamashita et al. (2010), Zhang et al. (2011), Zhang et al. (2012), Schiller et al. (2014), Sanborn et al. (2019), and Williams et al. (2020). ε^{50}Ti and ε^{54}Cr are defined as the mass-independent deviations in the ^{50}Ti/^{47}Ti and ^{54}Cr/^{52}Cr ratios from terrestrial standards in parts per 10^4. (For interpretation of the references to color in this figure legend, the reader is referred to the web version of this article.)

return missions, respectively (e.g., Hamilton et al., 2019; Kitazato et al., 2019; Lauretta et al., 2019). Similar formation conditions and/or anhydrous parent material for the CM and CO chondrite parent bodies have been suggested based on similarities in bulk elemental and O-isotope compositions (Kallemeyn and Wasson, 1981; Clayton and Mayeda, 1999; Weisberg et al., 2006; Kimura et al., 2020; Piralla et al., 2020) as well as chondrule and matrix olivine compositions (Frank et al., 2014; Schrader and Davidson, 2017). However, distinct parent body origins have been suggested based on differences in bulk chondrule compositions (Rubin and Wasson, 1986), mean chondrule sizes (Schrader and Davidson, 2017), abundances of FeO-poor relict grains (Schrader and Davidson, 2017), mean matrix abundances (Weisberg et al., 2006), cosmic-ray exposure ages (Eugster, 2003), Ti and Cr isotopic compositions (e.g., Warren, 2011; Sanborn et al., 2019), and the absence of breccias containing both CM and CO chondrite materials (Schrader and Davidson, 2017). Quantitative modeling of meteorite parent body formation locations has further suggested that the CM and CO chondrite parent bodies accreted in nearby regions of the solar protoplanetary disk at different times (Sugiura and Fujiya, 2014; Desch et al., 2018). The CM and CO chondrites define a similar trend in three-oxygen isotope space, and the gap between the CM and CO chondrite compositions is partially populated by C2-ungrouped chondrites and the anomalous CM chondrites that show similarities to both groups (Fig. 2). It is noted that Kimura et al. (2020) recently reported O-isotope compositions for three highly primitive CM chondrites, Asuka 12085, 12169, and 12236 (gray squares in Fig. 2) which extend the compositional range previously defined by the CM chondrites (blue squares in Fig. 2) and overlap with the ranges defined by the C2-ungrouped and anomalous CM chondrites. Oxygen-isotope analyses of these samples suggest that either (1) the CM and CO chondrites share a single heterogeneous parent body, or (2) distinct CM and CO chondrite parent bodies may have formed in a common isotopic reservoir in the solar protoplanetary disk.

CM and CO chondrites define distinct compositional fields in plots of ε^{50}Ti versus ε^{54}Cr, Δ^{17}O versus ε^{50}Ti, and Δ^{17}O versus ε^{54}Cr (e.g., Warren, 2011; Sanborn et al., 2019). Oxygen-isotope data have been previously measured for a limited number of ungrouped chondrites (e.g., Clayton and Mayeda, 1999; Jacquet et al., 2016), but the ε^{50}Ti and ε^{54}Cr isotopic compositions of those plotting in the compositional gap between CM and CO chondrites in three-oxygen isotope space have not yet been determined. The primary goal of this study is to evaluate the relationship between CM and CO chondrites by conducting combined analyses of Ti, Cr, and O isotopic compositions of ungrouped and anomalous chondrites that either (1) plot in the gap between CM and CO chondrites in three-oxygen isotope space (or, if O-isotope compositions have not been previously measured, have similar mineralogic and/or geochemical characteristics to those that do plot in this gap), or (2) have previously been documented as having similarities to the CM or CO chondrites. The ungrouped carbonaceous chondrites studied here with potential relationships to CM and CO chondrites include

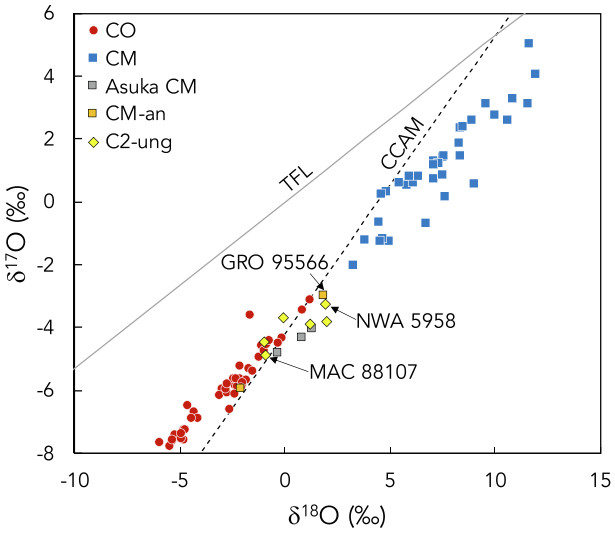

Fig. 2. Oxygen-isotope compositions of CO, CM, anomalous CM (CM-an), and C2-ungrouped (C2-ung) chondrites reported previously (Clayton and Mayeda, 1999; Greenwood and Franchi, 2004; Haack et al., 2012; Hewins et al., 2014; Jacquet et al., 2016; Lee et al., 2016, 2019; Alexander et al., 2018; Kimura et al., 2020); the data for the highly primitive CM chondrites, Asuka 12085, 12169, and 12236, are highlighted as the gray squares while all other CM data are shown as the blue squares. The terrestrial fractionation line (TFL; Clayton et al., 1973) and the line defining carbonaceous chondrite anhydrous minerals (CCAM; Clayton and Mayeda, 1977) are shown for reference. Arrows indicate three samples (GRO 95566, MAC 88107, and NWA 5958) included in the present study for which O-isotope compositions have been previously reported.

Elephant Moraine (EET) 83226, EET 83355, MacAlpine Hills (MAC) 87300, MAC 87301, MAC 88107, and Northwest Africa (NWA) 5958; the anomalous CM chondrite Grosvenor Mountains (GRO) 95566 was also analyzed.

The range of Ti and Cr isotopic compositions of the CM and CO chondrite groups are not well constrained. Therefore, we have measured the Ti and Cr isotopic compositions of Murchison (CM2), Murray (CM2), Aguas Zarcas (CM2), and Isna (CO3.8) to enable a more thorough comparison between the isotopic compositions of the ungrouped chondrites and the compositional ranges of the CM and CO chondrite groups. The paucity of Ti and Cr data for chondrites is a current limitation on making full use of these isotopic tracers as a tool for discriminating between different chondrite groupings. In particular, we wish to explore the extent to which the NC and CC groups are distinct. With this aim in mind, we have also measured Ti, Cr, and O isotopic compositions of several additional ungrouped chondrites with documented similarities to either the CC or NC groups, including LaPaz Ice Field (LAP) 04757 (chondrite-ung), LAP 04773 (chondrite-ung), Lewis Cliff (LEW) 85332 (C3-ung), and Coolidge (C4-ung). In total, we report here the Cr and Ti isotopic compositions for ten ungrouped chondrites, one anomalous CM chondrite, three CM chondrites, and one CO chondrite, as well as corresponding O-isotope compositions of nine of the ungrouped samples. Using these isotopic data, we assess potential genetic relationships between ungrouped chondrites and known chondrite groups, with a particular focus on evaluating the genetic relationship between CM and CO chondrites.

2. SAMPLES AND METHODS

2.1. Sample description

A total of 15 different meteorites were studied here (Table 1). Samples of nine meteorites were acquired from NASA's Antarctic Meteorite Collection. These samples, listed with their respective NASA split numbers following their sample names, are EET 83226,1, EET 83355,37, GRO 95566,34, LAP 04757,11, LAP 04773,7, LEW 85332,64, MAC 87300,77, MAC 87301,18, and MAC 88107,65. Samples of six meteorites were acquired from the Center for Meteorite Studies at Arizona State University (ASU). These

Table 1
List of the samples included in this study (2SD uncertainty for the elemental concentration values is ±5%).

Meteorite	Split Number	Classification	Mass Powdered (mg)	Mass Dissolved (mg)	Ti (ppm)	Cr (ppm)
EET 83226	1	C2-ung	133.2	19.26	875	4103
EET 83355	37	C2-ung	228.3	32.25	926	4687
MAC 87300	77	C2-ung	137.0	32.59	854	4297
NWA 5958	1743-3	C2-ung	523.2	35.45	1393	6980
LEW 85332	64	C3-ung	173.0	32.00	726	4493
MAC 88107	65	C3-ung	176.5	31.99	1357	6586
MAC 87301	18	C3-ung	198.5	44.20	611	2725
Coolidge	397.2x	C4-ung	778.3	31.20	1254	5500
LAP 04757	11	Chondrite-ung	160.8	28.97	834	5067
LAP 04773	7	Chondrite-ung	214.2	27.20	568	3622
GRO 95566	34	CM-an	133.0	32.44	682	3381
Aguas Zarcas A[1]	2121_5	CM2	82.6	64.35	1096	5600
Aguas Zarcas B[1]	2121_6	CM2	137.3	56.48	639	3212
Murchison	828,27	CM2	356.9	45.90	1176	5707
Murray	635,2	CM2	333.9	49.30	611	3156
Isna	984,1	CO3.8	548.5	49.70	872	4372

[1] Aguas Zarcas A is from the less altered lithology and Aguas Zarcas B is from the more altered lithology.

samples, listed with their respective ASU sample numbers, are Aguas Zarcas ("A" from 2121_5 and "B" from 2121_6), Coolidge (397.2x), Isna (984,1), Murchison (828,27), Murray (635,2), and NWA 5958 (1743-3).

2.2. Analytical methods

2.2.1. Sample digestion and concentration measurements

Interior samples (free of fusion crust) of Coolidge, EET 83226, EET 83355, GRO 95566, LAP 04757, LAP 04773, LEW 85332, MAC 87300, MAC 87301, MAC 88107, and NWA 5958 were crushed and powdered using a clean agate mortar and pestle in the Center for Meteorite Studies at ASU and aliquots of these sample powders were reserved for O-isotope analyses. Interior samples of Aguas Zarcas, Murchison, Murray, and Isna were crushed and powdered using a clean agate mortar and pestle in the Isotope Cosmochemistry and Geochronology Laboratory (ICGL) at ASU. In preparation for Cr and Ti isotopic analyses, all sample powders were digested in Parr bombs in a 2:1 ratio of concentrated HF and HNO_3 at 190 °C for >96 hours. These digested samples were then brought into solution in 6 N HCl and then dried down and brought into solution in 3% HNO_3. A ~5% aliquot of each sample solution was reserved for elemental concentration measurements using the Thermo Scientific iCAP-Q quadrupole inductively coupled plasma mass spectrometer in the Metals, Environmental and Terrestrial Analytical Laboratory (METAL) at ASU. Separate aliquots of the remaining ~95% of the sample solutions were then processed for Ti and Cr purification. Similar digestion procedures were used for the terrestrial rock standards BCR-2 and DTS-1 and the Smithsonian Allende CV (Vigarano-like) chondrite reference powder. Based on repeated analyses of standards, we estimate an uncertainty (2SD) of ±5% for elemental concentration measurements.

2.2.2. Titanium purification and isotopic analyses

An aliquot of each sample solution (equivalent to ~5–15 μg Ti) was chemically processed to obtain purified Ti following the methods of Torrano et al. (2019). The Ti yields exceeded 95% for all samples and standards with a procedural blank of less than 5 ng of Ti, which is insignificant compared to the total amount of Ti in the sample aliquots processed for Ti purification. Isotopic measurements of Ti were conducted on a Thermo Finnigan Neptune multi-collector inductively coupled plasma mass spectrometer (MC-ICPMS) in the ICGL at ASU using a jet sample cone and an H-skimmer cone in high-resolution mode (i.e., with a mass resolving power > 8000). Samples were introduced as solutions in 3% HNO_3 through a Cetac Aridus II desolvating nebulizer attached to a self-aspirating PFA with an uptake rate of 100 μL/min. An uptake time of 90 s and a wash time between consecutive sample and standard measurements of 120 s were used. Each repeat of a sample, standard, or blank comprised 50 cycles with an 8 s integration time per cycle. Purified Ti samples and standards were analyzed at a concentration of 1 ppm with a typical beam intensity for ^{48}Ti of ~25 V (on a faraday cup with a $10^{11}\Omega$ resistor). Titanium isotope data were collected by switching between two different cup configurations. The intensities of ^{44}Ca, ^{46}Ti, ^{47}Ti, ^{48}Ti, and ^{49}Ti were measured in the first cup configuration, followed by measurement of ^{47}Ti, ^{49}Ti, ^{50}Ti, ^{51}V, and ^{52}Cr intensities with the second cup configuration, with the intensities of ^{44}Ca, ^{51}V, and ^{52}Cr used to correct for isobaric interferences on the Ti masses. The Ca/Ti, V/Ti, and Cr/Ti ratios were measured for each sample solution prior to isotopic analyses to ensure that these ratios were below the maximum thresholds established by Zhang et al. (2011).

All data reduction, including blank correction, mass fractionation correction, and interference correction, was performed offline. The mass-independent Ti isotopic compositions are reported relative to the NIST 3162a Ti standard after correction for instrumental and natural mass-dependent fractionation using sample-standard bracketing and internal normalization to $^{49}Ti/^{47}Ti$ applying an exponential mass fractionation law and a $^{49}Ti/^{47}Ti$ ratio of 0.749766 (Niederer et al., 1981). Isotopic compositions are reported in ε notation, i.e., parts per ten thousand deviation from the standard. To assess the accuracy and precision of our methodology for Ti isotopic analyses (including chemical separation and mass spectrometry), we analyzed purified Ti from the BCR-2 terrestrial rock standard alongside samples during each analytical session. The mass-independent variations in Ti isotope ratios for BCR-2 reported here are within the uncertainties of zero and in agreement with previously reported data from other studies, including those which used different Ti bracketing standards (e.g., Zhang et al., 2011; Gerber et al., 2017; Davis et al., 2018; Render et al., 2019). Our external reproducibility based on repeat measurements of standards in our laboratory is ±0.15 (2SD) for $\varepsilon^{50}Ti$ (Supplementary Fig. EA2).

2.2.3. Chromium Purification via Column Chromatography

An aliquot of each sample solution (equivalent to ~5–15 μg Cr) was chemically processed to obtain purified Cr. All Cr purification chemistry was conducted in the ICGL at ASU following the methods of Yamakawa et al. (2009) with modifications based on Larsen et al. (2016) to control Cr speciation and thereby improve Cr elution yields (Table 2). The Cr yields of all samples and standards exceeded 95% and the average total procedural blank was less than 1 ng of Cr, which is insignificant compared to the total amount of Cr in the sample aliquots processed for Cr purification. Briefly, the first column separated Fe from other elements and used 1 mL of pre-cleaned Bio-Rad AG1-X8 200–400 mesh anion resin loaded onto a Bio-Rad polypropylene column (h = 42 mm, d = 5.5 mm). The sample was loaded onto the column in 1 mL of 6 M HCl and Cr was eluted immediately in 5 mL of 6 M HCl, along with Ni, Na, Ti, V, Mg, Ca, and Al. The final steps in this column removed Fe (in 8 mL of 0.5 M HCl) and Zn (in 6 mL of 3 M HNO_3). The second column separated Cr from Ni and rare earth elements (REEs) using 1 mL of Bio-Rad AG50W-X8 200–400 mesh anion resin loaded onto a Bio-Rad polypropylene column. The speciation of Cr in chloride form must be controlled to ensure proper elution of Cr on this column, as discussed by Larsen et al. (2016). In order to promote the formation of Cr(III)-Cl

Table 2
Cr purification procedure used in this study.

Column 1: AG1-X8, 200–400 mesh anion resin, 1 mL		
Step	Reagent	Volume (mL)
Condition Resin	3 M HNO_3	10
Condition Resin	MQ H_2O	18
Condition Resin	6 M HCl	12
Condition Resin	6 M HCl	6
Load Sample	6 M HCl	1
Elute Cr	6 M HCl	4
Elute Fe	0.5 M HCl	8
Elute Zn	3 M HNO_3	6
Column 2: AG50W-X8, 200–400 mesh cation resin, 1 mL		
Step	Reagent	Volume (mL)
Condition Resin	6 M HCl	16
Condition Resin	MQ H_2O	32
Load Sample	1 M HCl	2.4
Elute Cr	1 M HCl	4.6
Strip Column	6 M HCl	8
Column 3: AG50W-X8, 200–400 mesh cation resin, 0.3 mL		
Step	Reagent	Volume (mL)
Condition Resin	6 M HCl	9
Condition Resin	MQ H_2O	12
Load Sample	0.5 M HNO_3	3
Elute Na, Ti, V	0.5 M HNO_3	1
Elute Na, Ti, V	0.5 M HF	3
Elute Na, Ti, V	1 M HCl	5
Elute Cr	6 M HCl	5
Fe removal: AG1-X8 20–50 mesh anion resin, ~10 beads		
Step	Reagent	Volume (mL)
Fe Removal	10 M HCl	0.100

complexes, samples were fluxed on the hot plate in ~0.2 mL of concentrated HCl for 5 h at 120 °C (with sample solutions slowly rolled every ~20 minutes to ensure all solution remained in a bead at the bottom of the Teflon beaker) prior to loading on the second column. Once removed from the hot plate, sample solutions were diluted with MQ H_2O to make 2.4 mL of 1 M HCl and immediately loaded on the second column. The Cr was eluted in 7 mL of 1 M HCl, and remaining elements were eluted in 8 mL of 6 M HCl. The third column further purified Cr from remaining elements including Na, Ti, and V, using 0.3 mL of Bio-Rad AG50W-X8 200–400 mesh cation resin loaded onto a column made from a heat shrink Teflon tube (h = 23.3 mm, d = 4.05 mm). The speciation of Cr is also important for this column, so all samples were first placed in 1.5 mL of 1 M HNO_3 and heated in an oven at 50 °C for 24 h. Samples were then removed from the oven, diluted with MQ H_2O to make 3 mL of 0.5 M HNO_3, and immediately loaded onto the column. After elution of Na, Ti, and V (and other remaining elements) in 0.5 M HNO_3, 0.5 M HF, and 1 M HCl, Cr was eluted in 5 mL of 6 M HCl.

Total removal of Fe is critically important for accurate high-precision measurement of Cr isotope ratios (specifically $^{54}Cr/^{52}Cr$) using MC-ICPMS because ^{54}Fe is a direct isobaric interference on ^{54}Cr. Any residual Fe originating from the sample that is not completely separated during column chemistry is likely to be isotopically fractionated with $\delta^{56}Fe < 0$ (Anbar et al., 2000), complicating the ability to accurately account for the interference of ^{54}Fe on ^{54}Cr. Based on the results of our theoretical calculations (for a more detailed discussion, see Electronic Annex section EA.1), we proceeded with Cr isotopic analyses of our rock standards and samples only when $^{56}Fe/^{52}Cr < 5 \times 10^{-4}$ (measured via MC-ICPMS) was attained in the post-chemistry purified Cr solution. Because of the typical amount of Cr in our sample aliquots (~5–15 μg), achieving $^{56}Fe/^{52}Cr < 5 \times 10^{-4}$ requires a maximum of ~2.5–7.5 ng residual Fe depending on the sample. To ensure $^{56}Fe/^{52}Cr < 5 \times 10^{-4}$ for each sample prior to isotopic analyses, an additional post-column Fe-removal step was required. Following the third column, the sample Cr cuts were dried down and then brought into solution in 100 μL of 10 M HCL and approximately 10 beads of Bio-Rad AG1-X8 20–50 mesh anion resin were added. The sample beakers were then placed on an orbital shaker for 6 hours to ensure sufficient bead interaction with the solution. The sample solutions were then pipetted out of the beaker containing the beads and added to new clean Teflon beaker.

This method reliably achieved $^{56}Fe/^{52}Cr < 5 \times 10^{-4}$ for all samples and standards.

2.2.4. Cr isotopic analyses

Chromium isotopic measurements were conducted on a Thermo Finnigan Neptune MC-ICPMS at ASU using a jet sample cone and an H-skimmer cone in high-resolution mode (i.e., with a mass resolving power > 8000). Samples were introduced as solutions in 3% HNO_3 through an Elemental Scientific Apex-Q desolvating system attached to a self-aspirating PFA with an uptake rate of 100 μL/min. An uptake time of 90 s and a wash time between consecutive sample and standard measurements of 120 s were used. Each run for a sample, standard, or blank comprised 36 cycles with an 8 s integration time per cycle. Purified Cr samples and standards were analyzed at 800 ppb concentration, and the ion beam intensity for ^{52}Cr was ~25 V (on a faraday cup with a $10^{11}\Omega$ resistor). The beam intensities of ^{50}Cr, ^{52}Cr, ^{53}Cr, and ^{54}Cr were measured, along with ^{49}Ti, ^{51}V, and ^{56}Fe to monitor and correct for isobaric interferences. All data reduction was performed offline.

Mass-independent Cr isotopic compositions are reported relative to the NIST SRM 979 Cr standard after correction for instrumental and natural mass-dependent fractionation using sample-standard bracketing and internal normalization to $^{50}Cr/^{52}Cr$ applying an exponential mass fractionation law and a $^{50}Cr/^{52}Cr$ ratio of 0.051859 (Shields et al., 1966). To assess the accuracy and precision of our methodology for Cr isotope analyses (including chemical separation and mass spectrometry), we purified and measured the Cr isotopic compositions of the DTS-1 terrestrial rock standard and the Smithsonian Allende CV chondrite reference powder alongside samples. Isotopic compositions are reported in ε notation, i.e., parts per ten thousand deviation from the standard. Our external reproducibility (2SD) based on repeat measurements of pure Cr standards as well as terrestrial and meteoritic standards in our laboratory is ±0.13 for $\varepsilon^{54}Cr$ (Supplementary Fig. EA3).

2.2.5. Oxygen isotopic analyses

Oxygen-isotope analyses were performed (on aliquots of sample powders prepared at ASU, as described earlier in Section 2.2.1) at the Open University using an infrared laser-assisted fluorination system (Miller et al., 1999; Greenwood et al., 2017). Samples and standards were weighed out into a Ni sample block, with each aliquot weighing approximately 2 mg. The block was loaded into a vacuum-tight chamber and heated to 70 °C under vacuum overnight to remove surface-bound moisture. The system was then flushed with BrF_5 to reduce the final blank level to <60 nmoles O_2. Oxygen was released from the samples by heating in the presence of BrF_5 using a 50 W infrared CO_2 laser. After fluorination, the released oxygen gas was purified by passing it through two cryogenic nitrogen traps and over a bed of heated KBr to remove any excess fluorine. Oxygen gas was analyzed using a MAT 253 dual inlet mass spectrometer. Oxygen isotopic results are reported in standard δ notation in per mil (‰), where $\delta^{18}O$ has been calculated as: $\delta^{18}O$ (‰) = $([^{18}O/^{16}O]_{sample}/[^{18}O/^{16}O]_{VSMOW} - 1) \times 1000$, and similarly for $\delta^{17}O$ using the $^{17}O/^{16}O$ ratio. The deviation from the terrestrial fractionation line, $\Delta^{17}O$, has been calculated as $\Delta^{17}O$ (‰) = $\delta^{17}O - 0.52 \times \delta^{18}O$. Overall system precision, as defined by replicate analyses of the internal obsidian standard, is: ±0.053‰ for $\delta^{17}O$; ±0.095‰ for $\delta^{18}O$; ±0.018‰ for $\Delta^{17}O$ (2σ) (Starkey et al., 2016).

3. RESULTS

3.1. Ti, Cr, and O isotopic compositions

The mass-independent variations in the $^{50}Ti/^{47}Ti$ and $^{54}Cr/^{52}Cr$ ratios in each of the samples measured here are shown in ε notation in Table 3 (other mass-independent Ti and Cr isotopic compositions are reported in the Electronic Annex in Supplementary Tables EA1 and EA2). Also shown are the Ti isotopic compositions of the BCR-2 terrestrial rock standard and the Cr isotopic compositions of the DTS-1 terrestrial rock standard and the Smithsonian Allende CV chondrite reference powder. Our data for the terrestrial rock standards do not show any isotopic anomalies outside of the uncertainties, and our Cr isotopic data for Allende are consistent with previously reported values (e.g., Shukolyukov and Lugmair, 2006; Trinquier et al., 2007; Qin et al., 2010; Williams et al., 2020). The Ti isotopic composition of Allende was not measured in this study. This is because we recently reported the mass-independent Ti isotopic composition of Allende using the same methods utilized here (Torrano et al., 2019), and the values we reported in that study are within the range previously reported in the literature. The O-isotope compositions of the samples measured here are shown in Table 4.

4. DISCUSSION

4.1. Constraining the range of Ti and Cr isotopic compositions for CM and CO chondrites

All previously reported literature data as well as the data reported here for $\varepsilon^{50}Ti$ and $\varepsilon^{54}Cr$ values of CM and CO chondrites are shown in Fig. 3. For $\varepsilon^{50}Ti$, the previously reported data for CM chondrites defined a narrow range from 2.84 ± 0.05 for Murray (Zhang et al., 2012) to 3.03 ± 0.23 for Murchison (average of several measurements, including some that overlap with the Murray value; Trinquier et al., 2009; Zhang et al., 2011). In this study, we report an $\varepsilon^{50}Ti$ value for lithology A of Aguas Zarcas (2.21 ± 0.18) that is slightly lower than previously reported CM chondrite values. We also report an $\varepsilon^{50}Ti$ value of 2.86 ± 0.23 for lithology B of Aguas Zarcas that is within error of CM chondrite values reported previously and illustrates the isotopic heterogeneity that can be present within individual carbonaceous chondrites, particularly brecciated ones with distinct lithologies like Aguas Zarcas. The $\varepsilon^{50}Ti$ values reported previously for CO chondrites ranged from 3.37 ± 0.09 for CO3.4 Ornans (Zhang et al., 2012) to 4.69 ± 0.12 for CO3.3 Felix (Trinquier at al., 2009). The fraction of the CO3.8 chondrite Isna analyzed here, with an $\varepsilon^{50}Ti$ value of 2.83 ± 0.15, extends the lower boundary

Table 3
The ε^{50}Ti and ε^{54}Cr values of the meteorite samples studied here, as well as of the Smithsonian Allende reference powder and the BCR-2 and DTS-1 terrestrial rock standards analyzed during the same analytical sessions as the meteorite samples. The reported error is either the internal error (2SE) based on the number of analyses (n) of each sample solution or the external reproducibility (2SD), whichever is larger.

Sample	Classification	ε^{50}Ti	n	ε^{54}Cr	n
EET 83226	C2-ung	4.25 ± 0.15	6	0.93 ± 0.13	6
EET 83355	C2-ung	3.11 ± 0.15	3	0.76 ± 0.13	6
MAC 87300	C2-ung	4.67 ± 0.15	3	0.71 ± 0.14	6
NWA 5958	C2-ung	3.34 ± 0.15	5	1.18 ± 0.16	6
LEW 85332	C3-ung	2.42 ± 0.15	3	1.23 ± 0.13	6
MAC 88107	C3-ung	3.03 ± 0.15	6	1.11 ± 0.15	6
MAC 87301	C3-ung	4.12 ± 0.15	3	0.83 ± 0.14	6
Coolidge	C4-ung	2.67 ± 0.15	6	0.59 ± 0.13	6
LAP 04757	Chondrite-ung	–0.19 ± 0.15	1	–0.33 ± 0.13	6
LAP 04773	Chondrite-ung	–0.54 ± 0.15	3	–0.46 ± 0.16	6
GRO 95566	CM-an	3.50 ± 0.15	3	0.92 ± 0.13	3
Aguas Zarcas A[1]	CM2	2.21 ± 0.18	6	0.98 ± 0.13	6
Aguas Zarcas B[1]	CM2	2.86 ± 0.23	6	0.88 ± 0.13	6
Murchison	CM2	2.81 ± 0.15	5	1.10 ± 0.15	6
Murray	CM2	2.67 ± 0.15	6	0.84 ± 0.13	6
Isna	CO3.8	2.83 ± 0.15	6	0.66 ± 0.14	6
Allende	CV3	–	–	0.87 ± 0.13	6
Allende	CV3	–	–	0.94 ± 0.13	11
DTS-1	Ter. Std.	–	–	0.06 ± 0.13	6
BCR-2	Ter. Std.	–0.04 ± 0.15	5	–	–
BCR-2	Ter. Std.	–0.03 ± 0.17	6	–	–

[1] Aguas Zarcas A is from the less altered lithology and Aguas Zarcas B is from the more altered lithology.

Table 4
The O-isotope compositions of the meteorite samples studied here.

Meteorite	Classification	δ^{17}O (‰)	1σ	δ^{18}O (‰)	1σ	Δ^{17}O (‰)	1σ
EET 83226	C2-ung	–3.23	0.07	0.16	0.23	–3.36	0.05
EET 83355	C2-ung	–7.44	0.21	–4.67	0.21	–5.01	0.10
MAC 87300	C2-ung	–6.74	0.15	–3.48	0.18	–4.93	0.05
LEW 85332	C3-ung	–2.34	0.49	–1.08	0.64	–1.76	0.16
MAC 88107	C3-ung	–5.52	0.10	–1.71	0.14	–4.63	0.03
MAC 87301	C3-ung	–6.49	0.16	–3.28	0.20	–4.79	0.06
Coolidge	C4-ung	–5.48	0.16	–2.00	0.15	–4.44	0.09
LAP 04757	Chondrite-ung	2.49	0.04	3.44	0.04	0.70	0.02
LAP 04773	Chondrite-ung	2.41	0.07	3.20	0.06	0.75	0.03

of the compositional range for CO chondrites and causes it to overlap with the compositions of several CM chondrites (Fig. 3A). A previous study had reported an ε^{50}Ti value for another fraction of Isna of 3.54 ± 0.07 (Trinquier et al., 2009), which did not overlap with CM chondrite compositions. As with the CM chondrite Aguas Zarcas discussed above, this demonstrates that resolvable isotopic heterogeneity can be present within individual carbonaceous chondrites.

For ε^{54}Cr, the data reported previously for CM chondrites defined a narrow range and extended from 0.93 ± 0.09 for Paris (Göpel et al., 2015) to 1.13 ± 0.21 for Murray (Shukolyukov and Lugmair, 2006). In this study, we report an ε^{54}Cr value of 0.84 ± 0.13 for Murray, which is marginally within error of the value reported previously for this meteorite. Similarly, the average ε^{54}Cr value of 0.99 ± 0.20 reported previously for Murchison (Trinquier et al., 2007; Qin et al., 2010) agrees within the uncertainties of the value reported here for this meteorite (1.10 ± 0.15). The two fractions of Aguas Zarcas analyzed here have ε^{54}Cr values that are within error of each other and fall within the range of previously reported data for CM chondrites (Fig. 3B). The Cr isotope data reported previously for CO chondrites suggested a greater degree of heterogeneity, with ε^{54}Cr values ranging from 0.57 ± 0.11 for Lancé (Trinquier et al., 2007) to 0.95 ± 0.21 for Kainsaz (Shukolyukov and Lugmair, 2006; Qin et al, 2010) (Fig. 3B). The ε^{54}Cr value reported here for Isna of 0.66 ± 0.14 falls within the range of previously reported data. As can be seen in Fig. 3, there is some apparent overlap

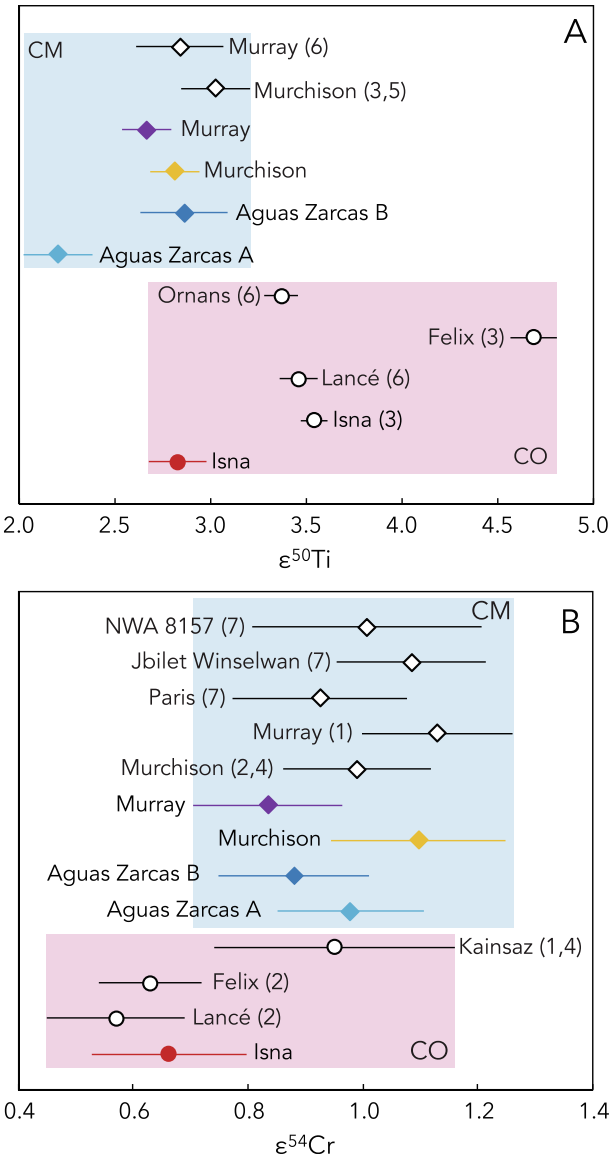

Fig. 3. Plots of (A) ε^{50}Ti and (B) ε^{54}Cr of CM and CO chondrites reported here (colored symbols) and those reported previously in the literature (open black symbols). Errors on the data from the present study are internal 2SE or external 2SD, whichever is larger. The data from previous literature (denoted by numbers in parentheses next to the meteorite names) represent the average (±2SD) values of ε^{50}Ti and ε^{54}Cr of individual meteorites for CM (Murchison, Murray, Paris, Jbilet Winselwan, and NWA 8157) and CO (Felix, Isna, Kainsaz, Lancé, and Ornans) chondrites, and are from: (1) Shukolyukov and Lugmair (2006); (2) Trinquier et al. (2007); (3) Trinquier et al. (2009); (4) Qin et al. (2010); (5) Zhang et al. (2011); (6) Zhang et al. (2012); and (7) Göpel et al. (2015). Shaded regions represent the compositional ranges of the CM (blue) and CO (pink) chondrites.

in the mass-independent Ti and Cr isotopic compositions of the CM and CO chondrites, but the overall ranges of each are defined by few samples.

Utilizing the mass-independent isotopic compositions of both Ti and Cr together may have the potential to better define differences between the CM and CO chondrites. Although the primary focus of this study is on the CM and CO chondrites and ungrouped chondrites potentially related to these two groups, it is important to consider the isotopic compositions of these samples in the context of all carbonaceous chondrite groups. In ε^{50}Ti versus ε^{54}Cr space, the compositional ranges for of all carbonaceous chondrite groups are in close proximity to each other and even overlap for some groups (Fig. 4). Nevertheless, an apparent inverse correlation between ε^{50}Ti and ε^{54}Cr is observed. The previously reported compositional ranges in ε^{50}Ti versus ε^{54}Cr space for different carbonaceous chondrite groups are defined by limited data (only one to three meteorites per group) where the Ti and Cr data were often obtained on separate aliquots of the same meteorites in different laboratories (see references to the literature data cited in the caption for Fig. 4).

Prior to this study, the compositional ranges in ε^{50}Ti versus ε^{54}Cr space for the CM and CO chondrite groups were defined by just two meteorites from each group for which the isotopic compositions of both Ti and Cr were reported (Fig. 4A). Furthermore, some of these previously reported Ti and Cr isotope compositions were measured in different laboratories on different fractions of these meteorites. In this work, we report mass-independent isotopic compositions for Ti and Cr (i.e., ε^{50}Ti and ε^{54}Cr) in the same solutions of each of three CM2 chondrites (Murray, Murchison, and Aguas Zarcas) and one CO3.8 chondrite (Isna). These new data are shown in Fig. 4B and extend the CM and CO chondrite compositional ranges compared to those that were reported previously (shown in Fig. 4A). The addition of four CM chondrite samples (from three distinct meteorites) and another CO chondrite sample significantly expands the compositional ranges of these carbonaceous chondrite groups in ε^{50}Ti versus ε^{54}Cr space (Fig. 4). The limited data reported thus far, as well as the fact that most previously reported mass-independent Ti and Cr isotopic compositions were obtained for separate sample aliquots of inherently heterogeneous meteorites, highlight the need for additional data to better constrain the compositional ranges of carbonaceous chondrite groups in ε^{50}Ti versus ε^{54}Cr space. This is essential for the use of these isotopic tracers to assess potential genetic relationships between such meteoritic samples.

4.2. Quantifying the potential effects of non-representative sampling on ε^{50}Ti and ε^{54}Cr

The variation in the Ti and Cr isotopic compositions among samples from the same chondrite group and even among different fractions of the same sample highlights both the importance and the difficulty of representatively sampling inherently heterogeneous samples. We have made an effort to measure sufficiently large sample sizes (Table 1), but because of the sample-limited nature of some meteorites this will continue to be an issue worthy of attention in studies that analyze and interpret bulk meteorite data. One potential source of Ti and Cr isotopic heterogeneity in analyses of bulk samples of some carbonaceous chondrites is the potentially millimeter- to centimeter-scale heterogeneity in the distribution of isotopically anomalous phases such as

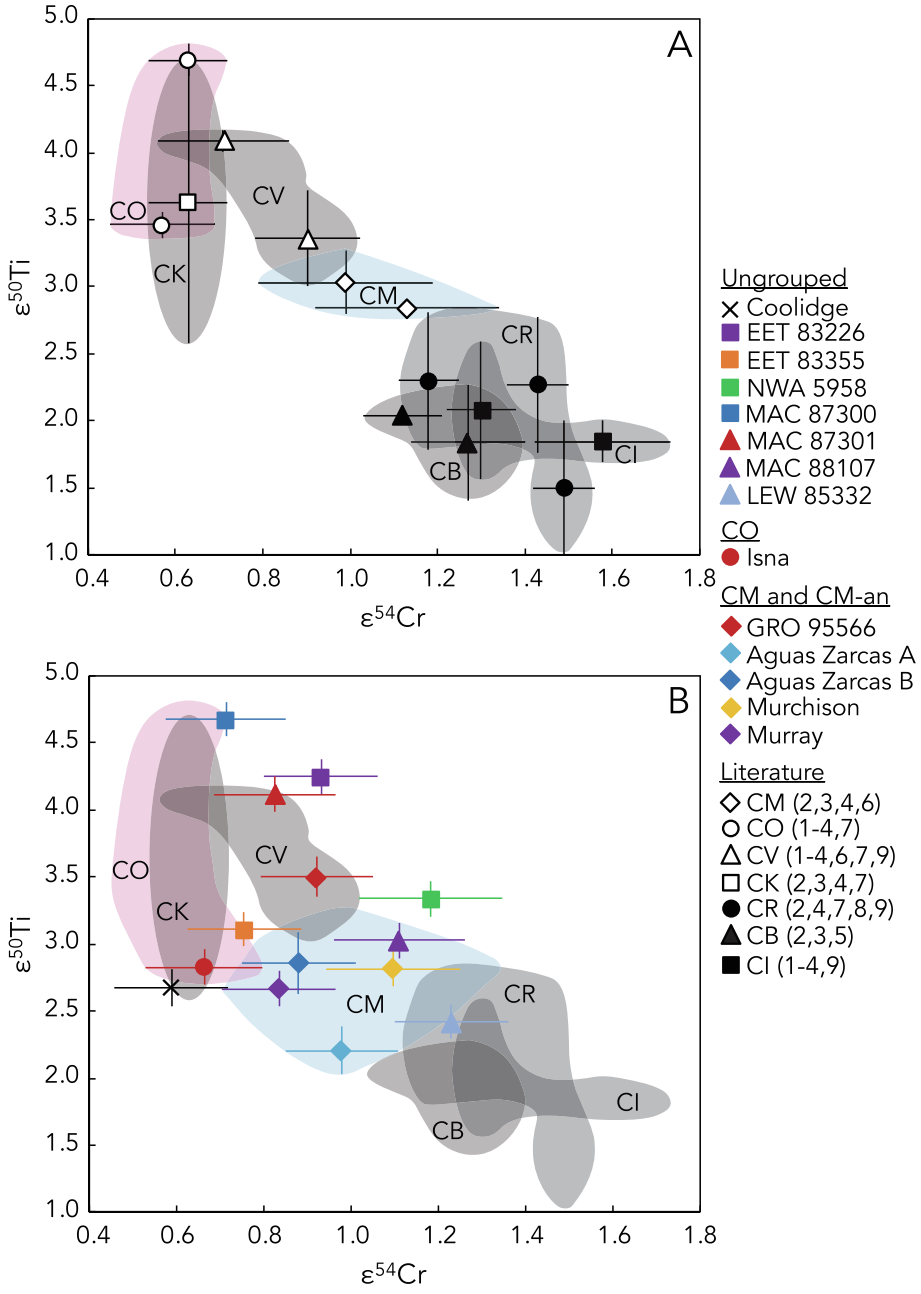

Fig. 4. (A) ε^{50}Ti versus ε^{54}Cr for bulk carbonaceous chondrites reported in the literature prior to this study (black and white symbols). These literature data points represent the average (±2SD) values of ε^{50}Ti and ε^{54}Cr of individual meteorites belonging to the CI (Ivuna-like), CB (Bencubbin-like), CR (Renazzo-like), CM, CO, CV, and CK (Karoonda-like) chondrite groups; note that both ε^{50}Ti and ε^{54}Cr data have been previously reported for only one to three meteorites from each carbonaceous chondrite group. Shaded and labeled regions represent the ranges for each of these carbonaceous chondrite groups in ε^{50}Ti versus ε^{54}Cr space; the pink region represents CO chondrites, the blue region represents CM chondrites, and all other chondrite groups are indicated by gray regions. Literature data, as denoted by corresponding numbers in parentheses in the legend, are from: (1) Shukolyukov and Lugmair (2006); (2) Trinquier et al. (2007); (3) Trinquier et al. (2009); (4) Qin et al. (2010); (5) Yamashita et al. (2010); (6) Zhang et al. (2011); (7) Zhang et al. (2012); (8) Sanborn et al. (2019); and (9) Williams et al. (2020). (B) ε^{50}Ti versus ε^{54}Cr for the bulk carbonaceous chondrites studied here (colored symbols). Error bars are internal 2SE or external 2SD, whichever is larger. As shown in (A) above, the gray regions are the ranges of literature data for CI, CB, CR, CV, and CK chondrites; the regions for the CM (blue) and CO (pink) chondrites are expanded as a result of the data reported in the present study. (For interpretation of the references to color in this figure legend, the reader is referred to the web version of this article.)

calcium-aluminum-rich inclusions (CAIs) and chondrules. The CAIs (median ε^{50}Ti of ~9 and median ε^{54}Cr of ~5; e.g., Dauphas and Schauble, 2016; Davis et al., 2018; Render et al., 2019; Torrano et al., 2019; and references therein) are likely to have a more significant effect than chondrules, which have ε^{50}Ti and ε^{54}Cr anomalies of a gen-

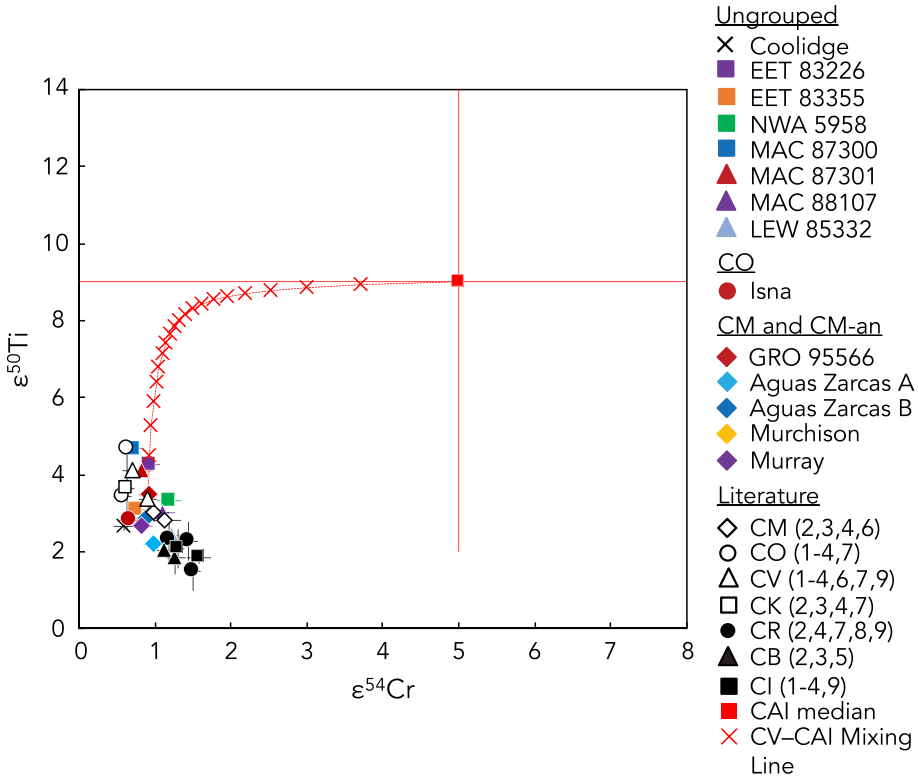

Fig. 5. The calculated mixing trend (red line, red crosses) in ε^{50}Ti versus ε^{54}Cr space between bulk Allende CV chondrite composition (white triangle, located at one end of the mixing trend) and median CAI composition (solid red square, located at the other end of the mixing trend), plotted with bulk carbonaceous chondrite data from this study (colored symbols) and from the literature (solid and open black symbols; numbers in parentheses correspond to the same references as in Fig. 4). The bulk Allende CV chondrite endmember of the mixing trend is the average defined by the elemental abundances (Cr = 3600, Ti = 899 ppm) and isotopic compositions (ε^{54}Cr = 0.90 ± 0.12, ε^{50}Ti = 3.36 ± 0.36) previously reported for Allende (e.g., Shukolyukov and Lugmair, 2006; Trinquier et al., 2007, 2009; Qin et al., 2010; Zhang et al., 2012; Alexander, 2019; Torrano et al., 2019). The CAI endmember of the mixing trend is defined by the mean elemental abundances (Cr = 418 ppm, Ti = 4218 ppm) in the CAIs studied by Torrano et al. (2019) and the median Cr and Ti isotopic compositions of CAIs from the literature (ε^{50}Ti = 9 and ε^{54}Cr = 5; e.g., Dauphas and Schauble, 2016 and references therein; Davis et al., 2018; Render et al., 2019; Torrano et al., 2019). Each red cross on the mixing trend represents a 5% incremental addition of the CAI-like composition to a bulk Allende composition. (For interpretation of the references to color in this figure legend, the reader is referred to the web version of this article.)

erally smaller magnitude (Olsen et al., 2016; Gerber et al., 2017; Schneider et al., 2020; Williams et al., 2020). The non-representative sampling of CAIs would also have a more significant effect on bulk ε^{50}Ti values compared to bulk ε^{54}Cr values because of the much higher elemental abundance of Ti compared to Cr in CAIs relative to the carbonaceous chondrite matrix. This effect is illustrated in Fig. 5, which shows that a ~5% oversampling of CAI material in the bulk Allende CV chondrite composition would be sufficient to cause a shift in ε^{50}Ti of ~1ε while ε^{54}Cr would remain largely unaffected. Much of the spread in ε^{50}Ti of representatively sampled bulk carbonaceous chondrites is likely because of the varying CAI abundances inherent in the different chondrite groups as documented by petrologic investigations (e.g., Weisberg et al., 2006 and references therein), but it is nevertheless important to consider the potential effects of non-representative sampling.

To assess the potential contribution of non-representative sampling of CAIs in the bulk samples studied here, we have compared their ε^{50}Ti values to their Ca and Al elemental abundances (which are taken as a proxy for CAI content) (Fig. 6). We have focused on paired samples or those for which multiple aliquots were measured to assess the implications of relative differences in elemental abundances and isotopic compositions in similar samples. If any of these measured samples oversampled isotopically anomalous CAI material, we would expect to see elevated Ca and Al elemental abundances correlated with an elevated ε^{50}Ti isotopic composition. Such a correlation is observed between the paired samples MAC 87301 and MAC 87300, with an increase in both Ca and Al abundances of ~0.5 wt.% for MAC 87300 corresponding to an increase in ε^{50}Ti of ~0.5. Such a ~0.5 wt.% increase in Ca and Al abundances could theoretically be accounted for by a ~5–10% oversampling of CAI material, which would cause a predicted increase in ε^{50}Ti of ~0–1 depending on the isotopic composition of the CAI material, consistent with the ε^{50}Ti values measured in these samples. However, it should be considered that such a correlation between Ca and Al abundances and ε^{50}Ti may simply reflect natural variations in elemental abundances and isotopic compositions of bulk meteorites. No correlation

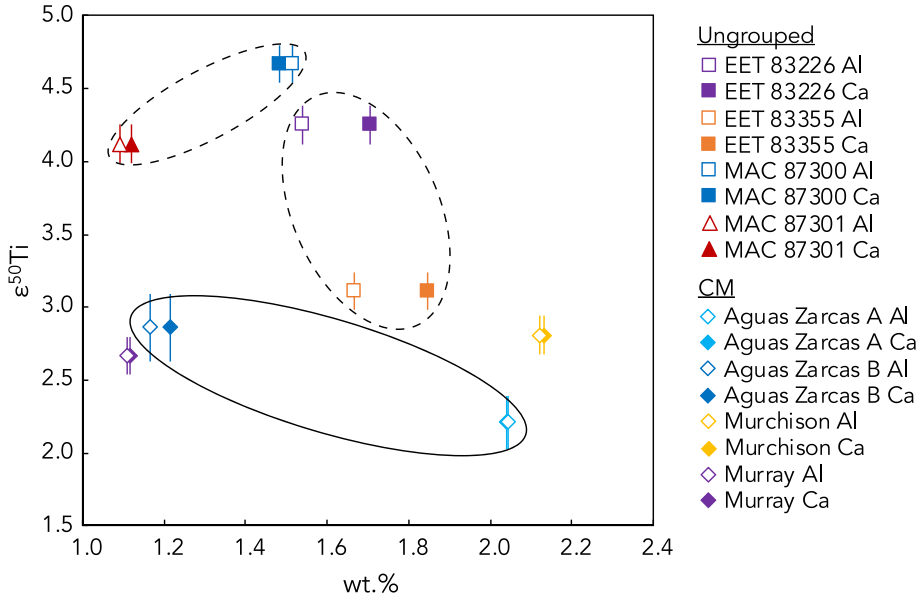

Fig. 6. ε^{50}Ti versus weight percent (wt.%) for eight samples studied here, with wt.% Al indicated by open symbols and wt.% Ca indicated by filled symbols. The dashed ovals include paired meteorites EET 83226/83355 and MAC 87300/87301 and the solid oval includes multiple aliquots of Aguas Zarcas. Error bars are internal 2SE or external 2SD, whichever is larger.

between Ca and Al abundances and ε^{50}Ti is observed for the paired samples EET 83355 and EET 83226, and an inverse correlation is observed for two aliquots of Aguas Zarcas, suggesting that oversampling of CAIs was not a factor in the ε^{50}Ti variation between these samples (Fig. 6). Furthermore, the Murray and Murchison CM chondrite samples show a ~1 wt.% difference in Ca and Al abundances but their ε^{50}Ti values are the same within error (Fig. 6). Additionally, a general lack of correlation between Ca and Al abundances and ε^{50}Ti values is observed in the sample set as a whole. All bulk carbonaceous chondrites measured here exhibit Ca and Al abundances of ~1–2.5 wt.%, and our results suggest that most such variation is caused by natural heterogeneity in their bulk chemistries and not by oversampling of CAIs. However, our calculations of the potential effect of oversampling of CAIs on ε^{50}Ti values (Fig. 6) emphasize the necessity of careful sampling practices to ensure representative analyses of bulk carbonaceous chondrites.

4.3. Using Ti, Cr, and O isotopes to evaluate potential genetic relationships

Previous studies have shown that the Ti, Cr, and O isotopic compositions of bulk meteorites can be used together as powerful tracers for establishing genetic links and identifying members of common chondrite groups (e.g., Warren, 2011; Sanborn et al., 2019). Here we use the combined isotopic compositions of Ti, Cr, and O to assess potential genetic relationships between the CM, CO, and ungrouped and anomalous chondrites analyzed in this study (Figs. 7 and 8). It is noted that only those samples for which isotopic data exist for all three elements (i.e., Ti, Cr, and O) are plotted in Fig. 8. Therefore, the compositional ranges for the various carbonaceous chondrite groups in Fig. 8 do not represent the full range of O-isotope compositions that have been measured for these groups (for example, for the CM and CO chondrites; Fig. 2). As such, future Ti and Cr data for carbonaceous chondrites for which O-isotope data have been previously determined may significantly alter the compositional ranges shown here in plots of Δ^{17}O versus ε^{50}Ti and Δ^{17}O versus ε^{54}Cr (Fig. 8).

4.3.1. EET 83355 and EET 83226

EET 83355 is a C2-ungrouped carbonaceous chondrite that was suggested to be a heated CM chondrite based on bulk H, C, and N abundances (Alexander et al., 2013), but subsequent work revealed differences from the CM chondrites, including lower phyllosilicate abundance (Garenne et al., 2014) and systematically lower carbonate C contents and carbonate δ^{13}C values (Alexander et al., 2015). This sample plots within the CO chondrite field in ε^{50}Ti versus ε^{54}Cr space (Fig. 4) and three-oxygen isotope space (Fig. 7) and has a Δ^{17}O composition close to that of previously measured CO chondrites (Fig. 8). Both its ε^{54}Cr and ε^{50}Ti values overlap with those defined by the CM chondrite region.

EET 83355 exhibits similarities to EET 83226, suggesting that they may be paired (Grossman, 1994). In ε^{50}Ti versus ε^{54}Cr space, EET 83226 plots outside of any known carbonaceous chondrite group, with an elevated ε^{50}Ti similar to the CO, CV, and CK chondrites, and ε^{54}Cr similar to the CO, CM, and CV chondrites (Fig. 4). EET 83226 plots in the CM field in Δ^{17}O versus ε^{54}Cr space (Fig. 8B), but outside of known fields for carbonaceous chondrite groups in Δ^{17}O versus ε^{50}Ti space (Fig. 8A), and in the CO, CV, and CK fields in three-oxygen isotope space (Fig. 7). Its ε^{50}Ti and Δ^{17}O values are distinct from EET 83355, while its ε^{54}Cr is

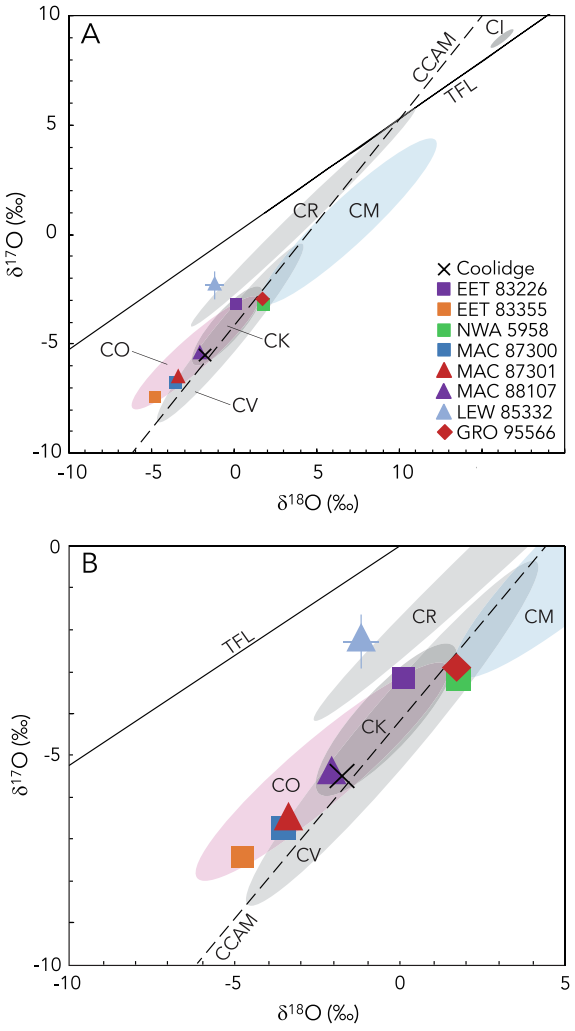

Fig. 7. Three-oxygen isotopic diagram showing data for bulk samples of the ungrouped and anomalous carbonaceous chondrites. The samples studied here include Coolidge, EET 83226, EET 83355, MAC 87300, MAC 87301, MAC 88107, and LEW 85332; also shown are the previously reported values for GRO 95566 (Clayton and Mayeda, 1999) and NWA 5958 (Jacquet et al., 2016). Panels A and B show the same data, with Panel B zoomed in to more clearly show the data reported in this study. Shaded regions indicate the ranges of previously reported data for the CI (Clayton and Mayeda, 1999), CM (Clayton and Mayeda, 1999; Haack et al., 2012; Hewins et al., 2014), CO (Clayton and Mayeda, 1999; Greenwood and Franchi, 2004; Alexander et al., 2018), CR (Weisberg et al., 1993; Clayton and Mayeda, 1999; Martins et al., 2007; Schrader et al., 2011, 2014), CK (Clayton and Mayeda, 1999; Greenwood et al., 2010), and CV (Clayton and Mayeda, 1999; Greenwood et al., 2010) chondrites. The terrestrial fractionation line (TFL; Clayton et al., 1973) and the line for carbonaceous chondrite anhydrous minerals (CCAM; Clayton and Mayeda, 1977) are plotted for reference.

elevated but within error of EET 83355. In three-oxygen isotope space, EET 83355 and EET 83226 plot at opposite ends of the CO chondrite compositional field, suggesting that EET 83355 may be less aqueously altered than EET 83226. If EET 83355 and EET 83226 do share a common parent body, these isotopic compositions suggest that such a parent body may have been isotopically heterogeneous with a composition similar to CO chondrites.

4.3.2. MAC 87300, MAC 87301, and MAC 88107

MAC 87300 (C2-ung), MAC 87301 (C3-ung), and MAC 88107 (C3-ung) make up a grouplet with bulk chemical compositions intermediate between those of CO and CM chondrites (Weisberg et al., 2006), high thermoluminescence compared to CM chondrites (Weisberg et al., 2006), and O-isotope compositions similar to CK chondrites (Clayton and Mayeda, 1999). These meteorites have undergone minimal parent body alteration and were all initially classified as C2 chondrites (Satterwhite and Mason, 1988; Martinez and Mason, 1989). It has also been suggested that MAC 87300 is related to heated CM, CR, and CI chondrites based on its similar, albeit more Fe-rich, matrix composition (Zolensky et al., 1993). The primary mineralogy of CAIs in MAC 87300 and MAC 88107 supports a relationship with the CO3 chondrites, although the presence of phyllosilicates suggests that CAIs from these meteorites have experienced a greater degree of aqueous alteration than that experienced by the CO3 chondrites (Russell et al., 2000).

In ε^{50}Ti versus ε^{54}Cr space, MAC 87300 falls within the CO chondrite field close to the CO3.3 chondrite Felix (Trinquier et al., 2009) and overlaps with ε^{54}Cr values for CM chondrite (Fig. 4). MAC 87301 exhibits an ε^{50}Ti value similar to CO chondrites and an ε^{54}Cr value similar to CM chondrites but that overlaps with CO chondrites (and with MAC 87300), suggesting characteristics intermediate between the CO and CM groups (Fig. 4). MAC 88107 falls in the CM chondrite region, with an elevated ε^{54}Cr compared to the CO chondrites, MAC 87300, and MAC 87301 (Fig. 4). MAC 87300 and MAC 87301 have very similar O-isotope compositions, and MAC 87300, MAC 87301, and MAC 88107 plot in the CO chondrite field in three-oxygen isotope space (Fig. 7) and near the CO field in plots of Δ^{17}O versus ε^{50}Ti and Δ^{17}O versus ε^{54}Cr (Fig. 8). These data are consistent with the pairing of MAC 87300 and MAC 87301. Furthermore, they suggest that MAC 87300 and MAC 87301 likely originated on a common parent body distinct from that of MAC 88107, and that both of these parent bodies formed from precursor material with isotopic similarities to the CO chondrites.

4.3.3. Coolidge

Coolidge is a C4-ungrouped carbonaceous chondrite that was initially thought to be related to the CV chondrites (Kallemeyn and Wasson, 1982). Subsequently, Kallemeyn and Rubin (1995) suggested that Coolidge is part of a distinct grouplet with Loongana 001 based on petrographic characteristics (such as matrix and chondrule abundances) and a bulk composition that is not consistent with known carbonaceous chondrite groups (specifically for Zn/Mn versus Al/Mn, Sb/Ni versus Ir/Ni, and Ga/Mg versus Sb/Mg). In ε^{50}Ti versus ε^{54}Cr space, Coolidge plots close to the CO chondrite field with an ε^{54}Cr value similar to the CO and CK chondrites and an ε^{50}Ti value that overlaps with CO,

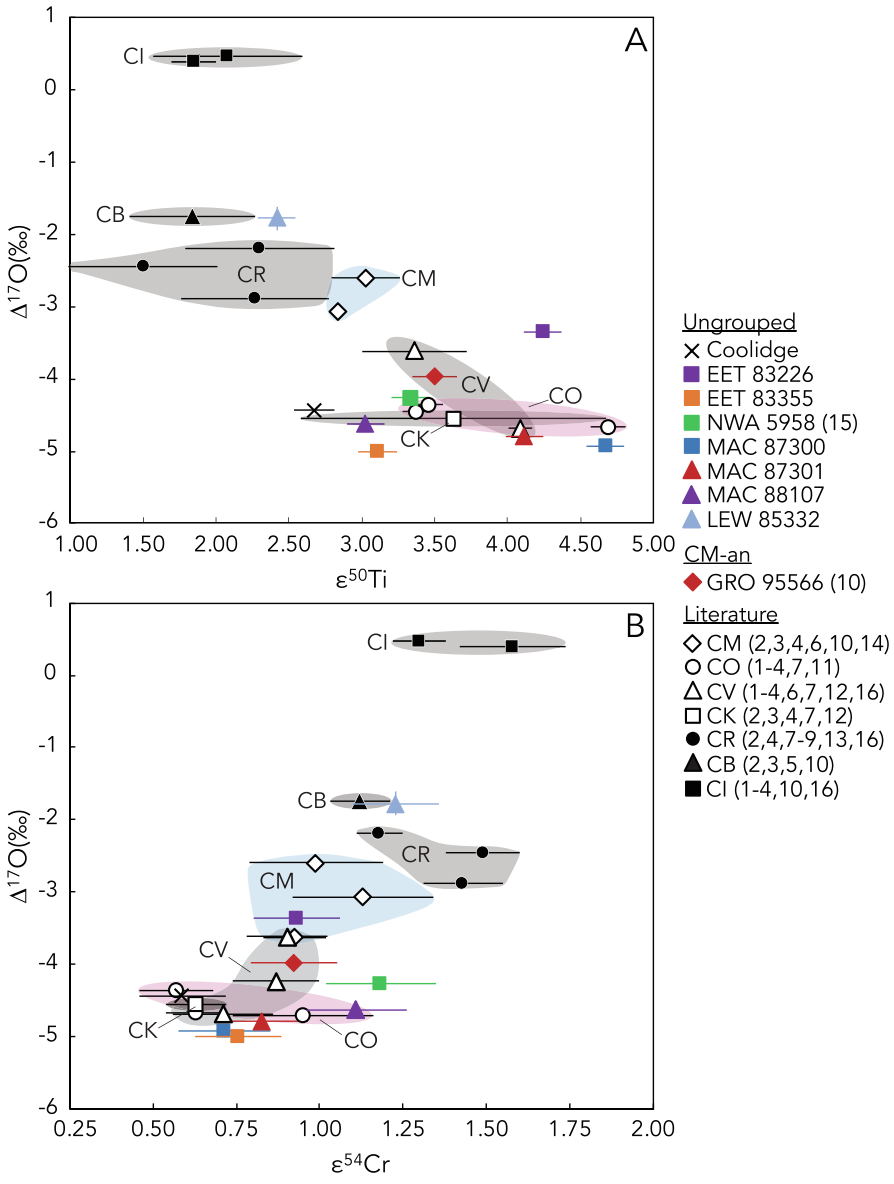

Fig. 8. Plots of (A) $\Delta^{17}O$ versus $\varepsilon^{50}Ti$ and (B) $\Delta^{17}O$ versus $\varepsilon^{54}Cr$ for bulk carbonaceous chondrite samples studied here and from the literature. The $\varepsilon^{50}Ti$ and $\varepsilon^{54}Cr$ data for Coolidge, EET 83226, EET 83355, NWA 5958, MAC 87300, MAC 87301, MAC 88107, LEW 85332, and GRO 95566 are from this study, as are the $\Delta^{17}O$ data for each of these samples except GRO 95566 (Clayton and Mayeda, 1999) and NWA 5958 (Jacquet et al., 2016). The $\Delta^{17}O$, $\varepsilon^{50}Ti$, and $\varepsilon^{54}Cr$ data for individual CM, CO, CV, CK, CR, CB, and CI chondrites measured previously are from: (1) Shukolyukov and Lugmair (2006); (2) Trinquier et al. (2007); (3) Trinquier et al. (2009); (4) Qin et al. (2010); (5) Yamashita et al. (2010); (6) Zhang et al. (2011); (7) Zhang et al. (2012); (8) Sanborn et al. (2019); (9) Weisberg et al. (1993); (10) Clayton and Mayeda (1999); (11) Greenwood and Franchi (2004); (12) Greenwood et al. (2010); (13) Schrader et al. (2011); (14) Hewins et al. (2014); (15) Jacquet et al. (2016); and (16) Williams et al. (2020), as denoted by the numbers in parentheses in the legend. Error bars are internal 2SE or external 2SD, whichever is larger.

CM, and CK chondrites (Fig. 4). Coolidge overlaps with the CO, CV, and CK compositional fields in three-oxygen isotope space (Fig. 7), and lies near CO, CV, and CK chondrites in plots of $\Delta^{17}O$ versus $\varepsilon^{50}Ti$ and $\Delta^{17}O$ versus $\varepsilon^{54}Cr$ (Fig. 8). These isotopic data suggest that Coolidge has similarities to multiple carbonaceous chondrite groups and should continue to be considered an ungrouped chondrite that originated on a parent body distinct from those of the known carbonaceous chondrite groups.

4.3.4. GRO 95566

GRO 95566 (CM-an) exhibits refractory lithophile abundances intermediate between the CV–CK and CM–CO chondrites, CM-like volatile lithophile abundances, refractory lithophile abundances similar to CM, CO, and CV chondrites, CM-like volatile siderophile and chalcophile abundances, lies within the CM field in a plot of Zn versus Sm concentrations, and plots between the CM and CO fields in Sb versus Ga concentrations (Choe

et al., 2010). The mean chondrule diameter of 310 μm (Choe et al., 2010) is similar to the ~300 μm mean diameter reported for CM chondrites (e.g., Friedrich et al., 2015). The O-isotope composition of GRO 95566 was previously reported by Clayton and Mayeda (1999) and it plots in the gap between CM and CO chondrites in three-oxygen isotope space (Figs. 2 and 7) and in its $\Delta^{17}O$ composition (Fig. 8). This O-isotope composition was a primary basis for its classification as an anomalous CM chondrite by Choe et al. (2010). GRO 95566 also has an intermediate composition between CM and CO chondrites in $\varepsilon^{50}Ti$ versus $\varepsilon^{54}Cr$ space (Fig. 4). In each of these isotope systems, such intermediate compositions also overlap with the CV chondrite fields (Figs. 4, 7, and 8). The combination of isotopic, elemental, and petrologic data suggests that GRO 95566 may represent minimally altered material on the CM parent body (Choe et al., 2010) or may originate from a distinct parent body formed from precursor material with a similar isotopic composition to CM and CO chondrites (potentially because it formed in a nearby region of the protoplanetary disk).

4.3.5. LEW 85332

LEW 85332 is a C3-ungrouped carbonaceous chondrite with similar refractory lithophile and siderophile abundances to the CI and CR chondrites and volatile siderophile abundances lower than CIs and higher than the CRs (Rubin and Kallemeyn, 1990). This sample also exhibits petrologic characteristics similar to the CO chondrites and was originally classified as a CO3 chondrite on the basis of its chondrule sizes (mean diameter = 170 μm; Mason, 1987; Rubin and Kallemeyn, 1990), which are similar to the mean values of 148 +132/–70 μm reported by Rubin (1989) for chondrules from CO chondrites. However, its refractory lithophile abundances and volatile siderophile abundances are inconsistent with those of CO or CM chondrites (Rubin and Kallemeyn, 1990). Additionally, matrix phyllosilicates suggest a relationship with CI and CR chondrites, but not with CM chondrites (Brearley, 1997). A relationship with the CR chondrites was also suggested based on previous O-isotope measurements of the bulk meteorite and individual chondrules (Clayton and Mayeda, 1999). Evidence that LEW 85332 is not a CR chondrite comes from its mean chondrule diameter of 170 μm (Rubin and Kallemeyn, 1990), which is significantly smaller than the mean diameter of ~700–1000 μm reported for CR chondrules (Bischoff et al., 1993; Kallemeyn et al., 1994; Rubin, 2000).

LEW 85332 lies in the CR chondrite field in plots of $\varepsilon^{50}Ti$ versus $\varepsilon^{54}Cr$ (Fig. 4) and $\Delta^{17}O$ versus $\varepsilon^{54}Cr$ (Fig. 8B), and near the CR field in three-oxygen isotope space (Fig. 7) and $\Delta^{17}O$ versus $\varepsilon^{50}Ti$ space (Fig. 8A). It $\varepsilon^{54}Cr$ and $\varepsilon^{50}Ti$ values also overlap with the CM chondrite field, suggesting that this sample may record compositional features that are intermediate between several chondrite groups. LEW 85332 is therefore best considered an ungrouped chondrite possessing similarities to multiple groups, and this sample illustrates the importance of conducting comprehensive combined petrologic, *in situ* chemical, bulk elemental, and isotopic analyses for the purpose of evaluating genetic relationships and parent body origins. The apparent disagreement of different data sets in identifying a parent body for LEW 85332 suggests that this sample may originate from one of perhaps many diverse carbonaceous chondrite parent bodies that are not represented by known chondrite groups. Such parent bodies may have formed from precursor materials that shared characteristics with multiple chondrite groups.

4.3.6. NWA 5958

NWA 5958 is a C2-ungrouped carbonaceous chondrite that exhibits depletion in moderately volatile elements similar to CM chondrites and an O-isotope composition that plots between the CM and CO chondrites in three-oxygen isotope space (Jacquet et al., 2016; Figs. 2 and 7). Based on petrographic and geochemical evidence, Jacquet et al. (2016) concluded that NWA 5958 is a CM-like C2-ungrouped chondrite that samples a parent body intermediate in composition between CM and CO chondrites. In $\varepsilon^{50}Ti$ versus $\varepsilon^{54}Cr$ space, NWA 5958 lies outside of any known carbonaceous chondrite group, with an $\varepsilon^{54}Cr$ value similar to CM chondrites and an $\varepsilon^{50}Ti$ value similar to CO chondrites (Fig. 4). In $\Delta^{17}O$ versus $\varepsilon^{54}Cr$ and $\Delta^{17}O$ versus $\varepsilon^{50}Ti$, NWA 5958 lies close to the CO chondrite field (Fig. 8). These data support the assertion of Jacquet et al. (2016) that NWA 5958 should be considered a CM-like C2-ungrouped chondrite.

4.3.7. LAP 04757 and LAP 04773

Approximately 90% of all classified meteorites fall within the H, L, and LL ordinary chondrite groups (Krot et al., 2013) based on characteristics such as bulk chemical and isotopic compositions and oxidation state (e.g., Rubin, 2005). Some ungrouped chondrites show similarities to ordinary chondrites but are compositionally inconsistent with belonging to one of the three recognized ordinary chondrite groups. Among these are those characterized by the low-FeO abundances of their mafic silicates compared to the range observed in most H chondrites, and these are referred to as the low-FeO chondrites (Russell et al., 1998). Several causes for the low-FeO nature of these meteorites were proposed by Wasson et al. (1993), including the incorporation of greater amounts of a reducing agent such as carbon, anomalous pressure and temperature conditions during metamorphism, and mixing with reducing agents in the parent body regolith. While Wasson et al. (1993) favored mixing with reducing agents on the parent body, subsequent studies suggested that the differences between the low-FeO chondrites and H chondrites were the result of the incorporation of distinct nebular materials and not parent body reduction of H chondrites (Russell et al., 1998; Troiano et al., 2011; Schrader et al., 2017a). Petrologic differences between low-FeO chondrites and H chondrites suggest that low-FeO chondrites may be derived from a distinct ordinary chondrite parent body (e.g., Troiano et al., 2011).

Two paired samples studied here, LAP 04757 and LAP 04773, are ungrouped chondrites that were initially thought to be related to the acapulcoites or low-FeO chondrites (Righter, 2007). Further study of LAP 04757 led to its identification as a low-FeO chondrite based on similarities to H

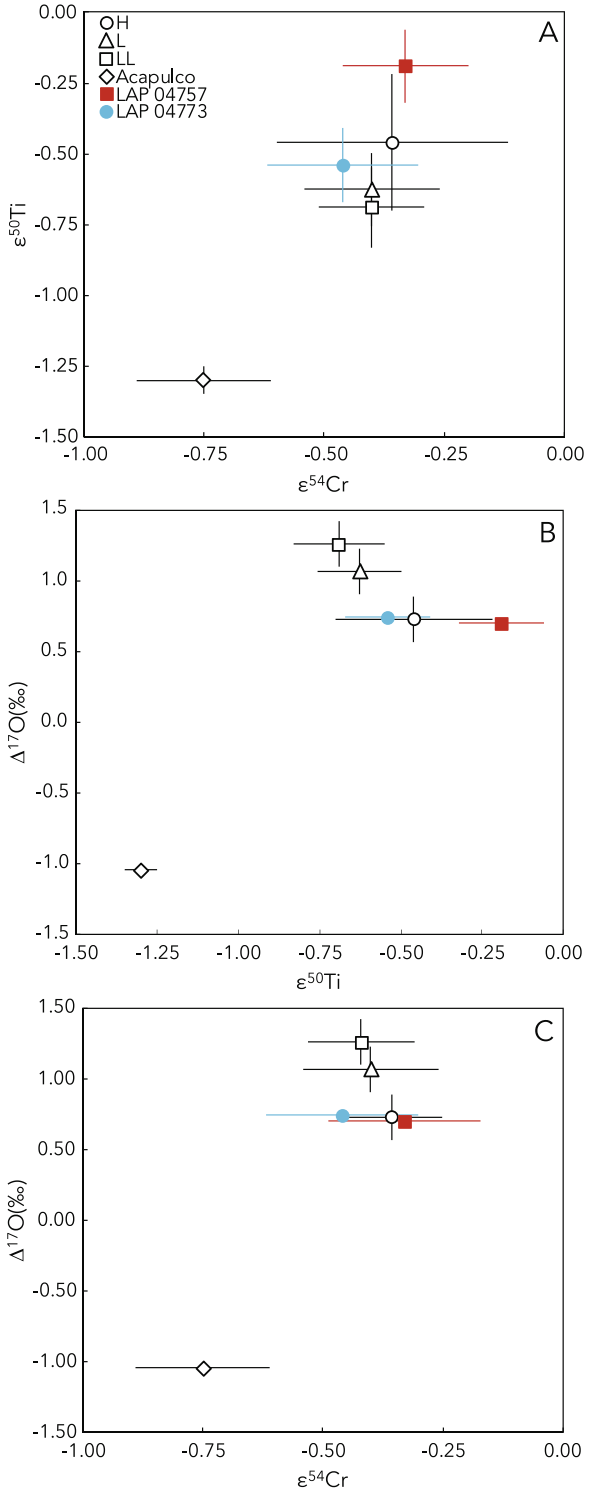

Fig. 9. Plots of (A) ε^{50}Ti versus ε^{54}Cr, (B) Δ^{17}O versus ε^{50}Ti, and (C) Δ^{17}O versus ε^{54}Cr showing data for LAP 04757 and LAP 04773 (from this study) along with literature values for Acapulco and H, L, and LL ordinary chondrites. The H, L, and LL data points represent mean ε^{50}Ti values reported previously from two H, three L, and four LL chondrites (Trinquier et al., 2009; Zhang et al., 2012), mean ε^{54}Cr values reported previously from four H, two L, and three LL chondrites (Trinquier et al., 2007; Qin et al., 2010; Schiller et al., 2014), and mean Δ^{17}O values from 22 H chondrites, 26 L chondrites, and 20 LL chondrites (Clayton et al., 1991). The Acapulco data point represents previously reported values for ε^{50}Ti (Zhang et al., 2012), ε^{54}Cr (Göpel et al., 2015), and Δ^{17}O (Clayton and Mayeda, 1996). Error bars are internal 2SE or external 2SD, whichever is larger.

chondrites in bulk elemental composition, siderophile abundances, lithophile abundances, moderately volatile element abundances, opaque mineral abundances, and O-isotope compositions (Troiano et al., 2011). Similarly, the paired LAP 04773 is also considered to be a low-FeO chondrite (e.g., Yamaguchi et al., 2019). In ε^{50}Ti versus ε^{54}Cr space, LAP 04773 plots within error of the H, L, and LL chondrites and LAP 04757 plots within error of the H chondrites (Fig. 9A). In plots of Δ^{17}O versus ε^{54}Cr and Δ^{17}O versus ε^{50}Ti, both samples overlap with the composition of H chondrites (Fig. 9B and 9C). LAP 04773 and LAP 04757 have clearly distinct isotopic compositions from Acapulco, confirming that they are unrelated to the acapulcoite group. These isotopic data provide support for the classification of LAP 04757 and LAP 04773 as low-FeO chondrites and suggest that these chondrites originated from a distinct parent body that may have formed from precursor materials with similar isotopic compositions, and from a similar formation region in the protoplanetary disk, as the H chondrite parent body.

4.4. Implications for the relationship between CM and CO chondrites

A close relationship between the CM and CO chondrites has been suggested based on bulk elemental and O-isotope compositions (e.g., Kallemeyn and Wasson, 1981; Clayton and Mayeda, 1999; Weisberg et al., 2006; Kimura et al., 2020; Piralla et al., 2020), and similar chondrule and matrix olivine compositions (Frank et al., 2014; Schrader and Davidson, 2017; Davidson et al., 2019). Although the gap in three-oxygen isotope space between CM and CO chondrites may be considered an argument against a common parent body origin, it could instead indicate a common parent body origin in which CO chondrites sample an anhydrous core, CM chondrites sample aqueously altered outer material, and CO-like and CM-like ungrouped chondrites sample an intermediate composition. Further isotopic analyses of individual bulk meteorites provide an additional means of evaluating this potential genetic relationship.

In ε^{50}Ti versus ε^{54}Cr and three-oxygen isotope plots, the CM and CO chondrites plot as adjacent but distinct fields (Figs. 2, 4, and 7); in plots of Δ^{17}O vs. ε^{54}Cr and Δ^{17}O vs. ε^{50}Ti, these two carbonaceous chondrite groups plot as clearly distinct fields separated by a larger gap (Fig. 7). As discussed by Schrader and Davidson (2017), the fact that the distinct ε^{54}Cr values of CM and CO chondrites are unaffected by aqueous alteration (unlike O-isotope compositions; e.g., Clayton and Mayeda, 1999;

Schrader et al., 2011, 2014) is evidence that they originated from distinct parent bodies and not on a single parent body that experienced different degrees of aqueous alteration.

The samples studied here that plot in the compositional gap between CM and CO chondrites in three-oxygen isotope space (NWA 5958 and GRO 95566; Fig. 2) lie outside the CM and CO chondrite fields in plots of ε^{50}Ti versus ε^{54}Cr (Fig. 4B), Δ^{17}O versus ε^{50}Ti (Fig. 8A), and Δ^{17}O versus ε^{54}Cr (Fig. 8B). The remaining ungrouped chondrites with documented similarities to the CM and/or CO chondrites largely plot outside the CM and CO fields in ε^{50}Ti versus ε^{54}Cr space, with one sample (EET 83355) overlapping both the CM and CO field, one (MAC 88107) plotting in the CM field, and one (MAC 87300) plotting in the CO field (Fig. 4). MAC 87301 lies near the CO field in plots of Δ^{17}O versus ε^{50}Ti (Fig. 8A) and Δ^{17}O versus ε^{54}Cr (Fig. 8B), while MAC 88107 plots in the CO field in Δ^{17}O versus ε^{54}Cr space (Fig. 8B) and EET 83226 plots in the CM field in Δ^{17}O versus ε^{54}Cr space (Fig. 8B). The remaining samples do not plot within the known CM or CO fields, although most lie closer to the CO field in plots of Δ^{17}O versus ε^{50}Ti and Δ^{17}O versus ε^{54}Cr (Fig. 8). No cluster of data exists between these fields, as might be expected if these samples represented intermediate compositions from a common CM–CO parent body. Instead, these data, combined with previous results of isotopic analyses, elemental abundance measurements, and petrologic investigations, suggest that the CM, CO, and related ungrouped chondrites likely originated from distinct parent bodies, some of which may have formed from isotopically similar precursor materials and in close proximity to each other in the protoplanetary disk. While Piralla et al. (2020) estimated the anhydrous O-isotope composition for CM and CO chondrites and showed that they may have had the same bulk anhydrous O-isotope compositions within uncertainties ($\Delta^{17}O = -3.97 \pm 1.19‰$ for CM vs. $-4.33 \pm 1.45‰$ for CO chondrites), the distinct Cr and Ti isotopic compositions between CM and CO chondrites identified in this study (Fig. 4) lead us to conclude that the CM and CO chondrites did not form from the same anhydrous materials. This conclusion is in agreement with Schrader and Davidson (2017) and Kimura et al. (2020), which also concluded that the CM and CO chondrites formed from similar but distinct starting materials.

4.5. Implications for the formation time and location of ungrouped chondrite parent bodies

A quantitative model predicting the heliocentric distance of meteorite parent body formation based on age constraints and refractory abundances predicts that the carbonaceous chondrite parent bodies formed at ~2–5 Ma after the beginning of the Solar System (as defined by the formation age of CAIs) outside the orbit of Jupiter beyond a pressure bump that prevented millimeter- and centimeter-sized particles from reaching the inner disk (Desch et al., 2018). This model predicts that the CO chondrite parent body formed at ~3.7 AU and ~2.7 Ma after the beginning of the Solar System, and the CM chondrite parent body formed later at ~3.7 AU and ~3.5 Ma. These parent body formation ages are based on previously reported Al-Mg ages of chondrules in CO and CM chondrites (Kurahashi et al., 2008), Mn-Cr ages of carbonate formation in CM chondrites (de Leuw et al. 2009; Fujiya et al. 2013; Jilly et al. 2014), timing of aqueous alteration in CM chondrites (Lee et al., 2012), and thermal modeling of CM and CO chondrite parent bodies (Sugiura and Fujiya, 2014); the estimates of heliocentric distances of formation of these parent bodies are based on refractory abundances (Scott and Krot, 2014). By comparison, the accretion location and formation time after the beginning of the Solar System are estimated to be ~3.6 AU and ~2.2 Ma for CK chondrites, ~3.6 AU and ~2.6 Ma for CV chondrites, ~3.8 AU and ~4.0 Ma for CR chondrites, and >15 AU and ~3.0 Ma for CI chondrites (Amelin et al., 2002; Hutcheon et al., 2009; Fujiya et al., 2013; Sugiura and Fujiya, 2014; Doyle et al., 2015; Nagashima et al., 2015; Budde et al., 2016; Bollard et al., 2017; Schrader et al., 2017b; Budde et al., 2018; Desch et al., 2018). The robustness of the Desch et al. (2018) model is supported by its accurate prediction of spectral matches to asteroid types and mean chondrule diameters. However, this model includes numerous assumptions and some free parameters, and its water content predictions for chondrite groups are contradicted by the recent finding that enstatite chondrites are not dry (Piani et al., 2020).

The predicted origin of CM and CO chondrites from distinct parent bodies that formed in regions separated spatially by <1 AU and temporally by ~0.8 Ma is consistent with the petrologic characteristics and isotopic compositions of these meteorites. In such a scenario, the ungrouped chondrites with documented similarities to CM and/or CO chondrites may therefore sample distinct parent bodies which formed at ~3.7 AU and ~2.7–3.5 Ma after the beginning of the Solar System, thus sampling precursor materials that were isotopically similar to those from which the CM and CO chondrites formed. The low-FeO chondrite parent body is thought to have formed from precursor material that was compositionally similar to the distinct H chondrite and IIE iron meteorite parent bodies (Bogard et al., 2000; Schrader and Davidson, 2017). It is predicted by the Desch et al. (2018) model that the H chondrite parent body formed near ~2.4 AU and at a time close to ~2.1 Ma, but the parent body of the IIE iron meteorites may have formed even earlier at <1 Ma after the beginning of the Solar System (Bogard et al., 2000). Therefore, according to this model, the parent body of the low-FeO chondrites LAP 04757 and LAP 04773 studied here may have formed at ~2.4 AU as late as ~2.1 Ma or as early as <1 Ma after the beginning of the Solar System.

4.6. Implications for asteroid sample return missions

The asteroids Bennu (B-type) and Ryugu (C-type) are the targets of the NASA OSIRIS-REx and JAXA Hayabusa2 sample return missions, respectively. The spectral properties and albedo measurements of these asteroids

share similarities with CM chondrites (e.g., Hamilton et al., 2019; Kitazato et al., 2019; Lauretta et al., 2019), but features similar to those of other chondrite groups are present as well. In the case of Bennu, a spectral feature at 0.55 μm is likely indicative of the presence of magnetite, which supports potential similarities with both CI and CM chondrites (Lauretta et al., 2019). In the case of Ryugu, no meteorites provide an exact match, but the closest analogs appear to be thermally metamorphosed CI chondrites and shock-heated CM chondrites (Kitazato et al., 2019). Additionally, spectra for Ryugu indicate the presence of Mg-rich phyllosilicates, which are known to be present in aqueously altered CI and CM chondrites (Kitazato et al., 2019). If Bennu and Ryugu are related to the CM chondrites, the Desch et al. (2018) model suggests that these asteroids likely formed near ~3.7 AU at approximately 3.5 Ma after the beginning of the Solar System. If these asteroids are instead related to CI chondrites, this would suggest formation at a heliocentric distance >15 AU and ~3.0 Ma (i.e., the suggested location and formation time of the CI chondrite parent body; Desch et al., 2018).

The results of our study demonstrate the compositional diversity of the carbonaceous chondrites, particularly among those that show similarities to the CM and CO chondrites. Isotopic data, combined with elemental abundances and petrologic characteristics, suggest that the CM, CO, and related ungrouped chondrites likely originated from distinct parent bodies that may have formed from isotopically similar precursor materials that likely originated in close proximity in the protoplanetary disk. Because initial data suggest that both Bennu and Ryugu are similar to the CM chondrites, it is possible that these asteroids formed from a similar nebular reservoir as parent bodies of the CM chondrites and the related ungrouped chondrites studied here. Therefore, the samples returned from Bennu and Ryugu are anticipated to provide important insights into the origins of such meteorites with the significant added benefit of geologic context. Detailed analyses of samples returned from these asteroids will also provide a test of the accuracy of meteorite analog predictions based on remote sensing and are likely to advance our ability to match carbonaceous chondrites in our collections to their parent asteroids.

5. CONCLUSIONS

In this study, we have reported the mass-independent isotopic compositions of Cr and Ti in three CM2 chondrites, one anomalous CM chondrite, one CO3.8 chondrite, and ten ungrouped chondrites. We have additionally reported the O-isotope compositions of a subset of these (i.e., nine of the ungrouped chondrites). The main conclusions of this work are as follows:

(1) The Cr and Ti isotopic compositions of three CM2 chondrites and one CO3.8 chondrite reported here refine the compositional ranges defined by the CM and CO chondrites in ε^{50}Ti versus ε^{54}Cr space. This highlights the need for additional data to better constrain the compositional ranges defined by these chondrite groups.

(2) The majority of the ungrouped carbonaceous chondrites studied here with documented similarities to the CM and/or CO chondrites lie outside the CM and CO group fields in plots of ε^{50}Ti versus ε^{54}Cr, Δ^{17}O versus ε^{50}Ti, and Δ^{17}O versus ε^{54}Cr, although most lie closer to the CO field in plots of Δ^{17}O versus ε^{50}Ti, Δ^{17}O versus ε^{54}Cr, and three-oxygen isotope compositions. These data suggest that the CM, CO, and related ungrouped chondrites (i.e., with similar petrographic and/or geochemical characteristics to CM or CO chondrites) likely originated from distinct parent bodies that may have formed from isotopically similar precursor materials in formation regions in close proximity to each other in the solar protoplanetary disk.

(3) The isotopic compositions of two ungrouped chondrites measured here, LAP 04757 and LAP 04773, support the classification of these meteorites as low-FeO ordinary chondrites and confirm that they are unrelated to the acapulcoites. These isotopic data also suggest that the low-FeO chondrites originated from a distinct parent body that may have formed from isotopically similar precursor materials and in a similar formation region to that of the H chondrite parent body in the protoplanetary disk.

(4) Quantitative modeling of the formation location of meteorite parent bodies has suggested that CO chondrites formed at ~3.7 AU and ~2.7 Ma, CM chondrites formed at ~3.7 AU and ~3.5 Ma, and H chondrites formed at ~2.4 AU and ~2.1 Ma after the beginning of the Solar System (Desch et al., 2018). In such a scenario, the ungrouped carbonaceous chondrites studied here with documented similarities to the CM and/or CO chondrites may originate from distinct parent bodies that formed near ~3.7 AU and at ~2.7–3.5 Ma, thus sampling materials similar to those that formed the CM and CO chondrite parent bodies. The low-FeO chondrites studied here may originate from a parent body that formed close to the formation region of the H chondrite parent body near ~2.4 AU and at ~2.1 Ma, or as early as the formation time of the IIE iron meteorite parent body at <1 Ma after the beginning of the Solar System.

(5) Remote-sensing data from spacecraft have shown that both Bennu and Ryugu may be similar to CM chondrites (e.g., Hamilton et al., 2019; Kitazato et al., 2019; Lauretta et al., 2019), but suggestions of potential relationships with other groups, such as CI chondrites, indicate that these asteroids may also be related to the ungrouped chondrites studied here that show similarities to multiple chondrite groups. The samples returned from Bennu and Ryugu by the OSIRIS-REx and Hayabusa2 missions, respectively, may therefore provide important insights into the origins of such meteorites.

Declaration of Competing Interest

The authors declare that they have no known competing financial interests or personal relationships that could have appeared to influence the work reported in this paper.

ACKNOWLEDGMENTS

US Antarctic meteorite samples are recovered by the Antarctic Search for Meteorites (ANSMET) program which has been funded by NSF and NASA, and characterized and curated by the Department of Mineral Sciences of the Smithsonian Institution and Astromaterials Curation Office at NASA Johnson Space Center. We thank the ASU Center for Meteorite Studies for providing samples of several meteorites for this study. We also thank Rebekah Hines and Vinai Rai for their assistance with sample processing and data collection in the ICGL at ASU. We recognize that there are additional unpublished data available in abstract form for some of the samples discussed here, but journal policy precludes their inclusion as references. This manuscript was improved by constructive reviews from three anonymous reviewers and the editorial expertise of Thorsten Kleine.

FUNDING

This work was supported by NASA grant NNH19ZDA005K to Z. T. and M. W. and NASA grant NNX15AH41G to M.W. Oxygen isotope research at the Open University is supported through a consolidated grant (ST/T000228/1) from the UK STFC agency.

APPENDIX A. SUPPLEMENTARY MATERIAL

Supplementary data to this article can be found online at https://doi.org/10.1016/j.gca.2021.03.004.

REFERENCES

Alexander C. M. O. D., Howard K. T., Bowden R. and Fogel M. L. (2013) The classification of CM and CR chondrites using bulk H, C and N abundances and isotopic compositions. *Geochim. Cosmochim. Acta* **123**, 244–260.

Alexander C. M. O. D., Bowden R., Fogel M. L. and Howard K. T. (2015) Carbonate abundances and isotopic compositions in chondrites. *Meteorit. Planet. Sci.* **50**, 810–833.

Alexander C. M. O. D., Greenwood R. C., Bowden R., Gibson J. M., Howard K. T. and Franchi I. A. (2018) A mutli-technique search for the most primitive CO chondrites. *Geochim. Cosmochim. Acta* **221**, 406–420.

Alexander C. M. O. D. (2019) Quantitative models for the elemental and isotopic fractionations in the chondrites: The carbonaceous chondrites. *Geochim. Cosmochim. Acta* **254**, 277–309.

Amelin Y., Krot A. N., Hutcheon I. D. and Ulyanov A. A. (2002) Lead Isotopic Ages of Chondrules and Calcium-Aluminum-Rich Inclusions. *Science* **297**, 1678–1683.

Anbar A. D., Roe J. E., Barling J. and Nealson K. H. (2000) Nonbiological Fractionation of Iron Isotopes. *Science* **288**, 126–129.

Bischoff A., Palme H., Ash R. D., Clayton R. N., Schultz L., Herpers U., Stöffler D., Grady M. M., Pillinger C. T., Spettel B., Weber H., Grund T., Endreß M. and Weber D. (1993) Paired Renazzo-type (CR) carbonaceous chondrites from the Sahara. *Geochim. Cosmochim. Acta* **57**, 1587–1603.

Bogard D. D., Garrison D. H. and McCoy T. J. (2000) Chronology and petrology of silicates from IIE iron meteorites: evidence of a complex parent body evolution. *Geochim. Cosmochim. Acta* **64**, 2133–2154.

Bollard J., Connelly J. N., Whitehouse M. J., Pringle E. A., Bonal L., Jørgensen J. K., Nordlund Å., Moynier F. and Bizzarro M. (2017) Early formation of planetary building blocks inferred from Pb isotopic ages of chondrules. *Sci. Adv.* **3**, e1700407.

Brasser R. and Mojzsis S. J. (2020) The partitioning of the inner and outer Solar System by a structured protoplanetary disk. *Nat. Astron.* **4**, 492–499.

Brearley A. J. (1997) Phyllosilicates in the matrix of the unique carbonaceous chondrite, LEW 85332 and possible implications for the aqueous alteration of CI chondrites. *Meteorit. Planet. Sci.* **32**, 377–388.

Budde G., Kleine T., Kruijer T. S., Burkhardt C. and Metzler K. (2016) Tungsten isotopic constraints on the age and origin of chondrules. *Proc. Natl. Acad. Sci. U. S. A.* **113**, 2886–2891.

Budde G., Kruijer T. S. and Kleine T. (2018) Hf-W chronology of CR chondrites: implications for the timescales of chondrule formation and the distribution of ^{26}Al in the solar nebula. *Geochim. Cosmochim. Acta* **222**, 284–304.

Choe W. H., Huber H., Rubin A. E., Kallemeyn G. W. and Wasson J. T. (2010) Compositions and taxonomy of 15 unusual carbonaceous chondrites. *Meteorit. Planet. Sci.* **45**, 531–554.

Clayton R. N., Grossman L. and Mayeda K. (1973) A component of primitive nuclear composition in carbonaceous meteorites. *Science* **182**, 485–488.

Clayton R. N. and Mayeda T. K. (1977) Correlated oxygen and magnesium isotope anomalies in Allende Inclusions, I: Oxygen. *Geophysical Research Letters* **4**, 295–298.

Clayton R. N., Mayeda T. K., Goswami J. N. and Olsen E. J. (1991) Oxygen isotope studies of ordinary chondrites. *Geochim. Cosmochim. Acta* **55**, 2317–2338.

Clayton R. N. (1993) Oxygen isotopes in meteorites. *Annu. Rev. Earth Planet. Sci.* **21**, 115–149.

Clayton R. N. and Mayeda T. K. (1996) Oxygen isotope studies of achondrites. *Geochim. Cosmochim. Acta* **60**, 1999–2017.

Clayton R. N. and Mayeda T. K. (1999) Oxygen isotope studies of carbonaceous chondrites. *Geochim. Cosmochim. Acta* **63**, 2089–2104.

Dauphas N. and Schauble E. A. (2016) Mass fractionation laws, mass-independent effects, and isotopic anomalies. *Annu. Rev. Earth Planet. Sci* **44**, 709–783.

Davidson J., Alexander C. M. O', Stroud R. M., Busemann H. and Nittler L. R. (2019) Mineralogy and petrology of Dominion Range 08006: A very primitive CO3 carbonaceous chondrite. *Geochim. Cosmochim. Acta* **265**, 259–278.

Davis A. M., Zhang J., Greber N. D., Hu J., Tissot F. L. H. and Dauphas N. (2018) Titanium isotopes and rare earth patterns in CAIs: Evidence for thermal processing and gas-dust decoupling in the protoplanetary disk. *Geochim. Cosmochim. Acta* **221**, 275–295.

De Leuw S., Rubin A. E., Schmitt A. K. and Wasson J. T. (2009) ^{53}Mn–^{53}Cr systematics of carbonates in CM chondrites: implications for the timing and duration of aqueous alteration. *Geochim. Cosmochim. Acta* **73**, 7433–7442.

Desch S., Kalyaan A. and Alexander C. M. O. D. (2018) The effect of Jupiter's formation on the distribution of refractory elements and inclusions in meteorites. *Astrophys. J. Suppl. Ser.* **238**, 31 pp.

Doyle P. M., Jogo K., Nagashima K., Krot A. N., Wakita S., Ciesla F. J. and Hutcheon I. D. (2015) Early aqueous activity on the ordinary and carbonaceous chondrite parent bodies recorded by fayalite. *Nat. Commun.* **6**, 7444.

Eugster O. (2003) Cosmic-ray exposure ages of meteorites and Lunar rocks and their significance. *Chem. Erde* **63**, 3–30.

Frank D. R., Zolensky M. E. and Le L. (2014) Olivine in terminal particles of Stardust aerogel tracks and analogous grain in chondrite matrix. *Geochim. Cosmochim. Acta* **142**, 240–259.

Friedrich J. M., Weisberg M. K., Ebel D. S., Biltz A. E., Corbett B. M., Iotzov I. V., Khan W. S. and Wolman M. D. (2015) Chondrule size and related physical properties: A compilation and evaluation of current data across all meteorite groups. *Chemie der Erde* **75**, 419–443.

Fujiya W., Sugiura N., Sano Y. and Hiyagon H. (2013) Mn–Cr ages of dolomites in CI chondrites and the Tagish Lake ungrouped carbonaceous chondrite. *Earth Planet. Sci. Lett.* **362**, 130–142.

Garenne A., Beck P., Montes-Hernandez G., Chiriac R., Toche F., Quirico E., Bonal L. and Schmitt B. (2014) The abundance and stability of "water" in type 1 and 2 carbonaceous chondrites (CI, CM and CR). *Geochim. Cosmochim. Acta* **137**, 93–112.

Gerber S., Burkhardt C., Budde G., Metzler K. and Kleine T. (2017) Mixing and transport of dust in the early solar nebula as inferred from titanium isotope variations among chondrules. *Astrophys. J.* **841**, L17–L23.

Göpel C., Birck J. L., Galy A., Barrat J.-A. and Zanda B. (2015) Mn-Cr systematics in primitive meteorites: insights from mineral separation and partial dissolution. *Geochim. Cosmochim. Acta* **156**, 1–24.

Greenwood R. C. and Franchi I. A. (2004) Alteration and metamorphism of CO3 chondrites: Evidence from oxygen and carbon isotopes. *Meteorit. Planet. Sci.* **39**, 1823–1838.

Greenwood R. C., Franchi I. A., Kearsley A. T. and Alard O. (2010) The relationship between CK and CV chondrites. *Geochim. Cosmochim. Acta* **74**, 1684–1705.

Greenwood R. C., Burbine T. H., Miller M. F. and Franchi I. A. (2017) Melting and differentiation of early-formed asteroids: The perspective from high precision oxygen isotope studies. *Chemie der Erde-Geochemistry* **77**, 1–43.

Grossman J. N. (1994) The Meteoritical Bulletin, No 76, 1994 January: the US Antarctic meteorite collection. *Meteoritics* **29**, 100–143.

Haack H., Grau T., Bischoff A., Horstmann M., Wasson J., Sørensen A., Laubenstein M., Ott U., Palme H., Gellissen M., Greenwood R. C., Pearson V. K., Franchi I. A., Gabelica Z. and Schmitt-Kopplin P. (2012) Maribo–a new CM fall from Denmark. *Meteorit. Planet Sci.* **47**, 30–50.

Hamilton V., Simon A., Christensen P., Reuter D., Clark B., Barucci A., Bowles N., Boynton W., Brucato J., Cloutis E., Connolly, Jr., H., Donaldson Hanna K., Emery J., Enos H., Fornasier S., Haberle C., Hanna R., Howell E., Kaplan H., Keller L., Lantz C., Li J.-Y., Lim L., McCoy T., Merlin F., Nolan M., Praet A., Rozitis B., Sandford S., Schrader D. L., Thomas C., Zou X.-D. and Lauretta OSIRIS-REx Team D. (2019) Evidence for widespread hydrated minerals on asteroid (101955) Bennu. *Nature Astronomy* **3**, 332–340.

Hewins R. H., Bourot-Denise M., Zanda B., Leroux H., Barrat J.-A., Humayun M., Gopël C., Greenwood R. C., Franchi I. A., Pont S., Lorand J.-P., Cournéde C., Gattacceca J., Rochette P., Kuga M., Marrocchi Y. and Marty B. (2014) The Paris meteorite, the least altered CM chondrite so far. *Geochim. Cosmochim. Acta* **124**, 190–222.

Hutcheon I. D., Marhas K. K., Krot A. N., Goswami J. N. and Jones R. H. (2009) ^{26}Al in plagioclase-rich chondrules in carbonaceous chondrites: Evidence for an extended duration of chondrule formation. *Geochim. Cosmochim. Acta* **73**, 5080–5099.

Jacquet E., Barrat J.-A., Beck P., Caste F., Gattacceca J., Sonzogni C. and Gounelle M. (2016) Northwest Africa 5958: A weakly altered CM-related ungrouped chondrite, not a CI3. *Meteorit. Planet. Sci.* **51**, 851–869.

Jilly C. E., Huss G. R., Krot A. N., Nagashima K., Yin Q.-Z. and Sugiura N. (2014) ^{53}Mn–^{53}Cr dating of aqueously formed carbonates in the CM2 lithology of the Sutter's Mill carbonaceous chondrite. *Meteorit. Planet. Sci.* **49**, 2104–2117.

Kallemeyn G. W. and Wasson J. T. (1981) The compositional classification of chondrites – I. The carbonaceous groups. *Geochim. Cosmochim. Acta* **45**, 1217–1230.

Kallemeyn G. W. and Wasson J. T. (1982) The compositional classification of chondrites: III. Ungrouped carbonaceous chondrites. *Geochim. Cosmochim. Acta* **46**, 2217–2228.

Kallemeyn G. W., Rubin A. E. and Wasson J. T. (1994) The compositional classification of chondrites: VI. The CR chondrite group. *Geochim. Cosmochim. Acta* **58**, 2873–2888.

Kallemeyn G. W. and Rubin A. E. (1995) Coolidge and Loongana 001: a new carbonaceous chondrite grouplet. *Meteoritics* **30**, 20–27.

Kimura M., Imae N., Komatsu M., Barrat J. A., Greenwood R. C., Yamaguchi A. and Noguchi T. (2020) The most primitive CM chondrites, Asuka 12085, 12169, and 12236, of subtypes 3.0–2.8: Their characteristic features and classification. *Polar Sci.* **26**, 100565.

Kitazato K., Milliken R. E. and Iwata T., et al. (2019) The surface composition of asteroid 162173 Ryugu from Hayabusa2 near-infrared spectroscopy. *Science* **364**, 272–275.

Krot A. N., Keil K., Scott E. R. D., Goodrich C. A. and Weisberg M. K. (2013) Classification of meteorites and their genetic relationships. In *Treatise on Geochemistry* (eds. H. D. Holland and K. K. Turekian), vol. 1, second ed. Elsevier, Oxford, pp. 1–63.

Kruijer T. S., Burkhardt C., Budde G. and Kleine T. (2017) Age of Jupiter inferred from the distinct genetics and formation times of meteorites. *Proc. Natl. Acad. Sci.* **114**, 6712–6716.

Kruijer T. S., Kleine T. and Borg L. E. (2020) The great isotopic dichotomy of the early Solar System. *Nat. Astron.* **4**, 32–40.

Kurahashi E., Kita N. T., Nagahara H. and Morishita Y. (2008) ^{26}Al–^{26}Mg systematics of chondrules in a primitive CO chondrite. *Geochim. Cosmochim. Acta* **72**, 3865–3882.

Larsen K. K., Wielandt D., Schiller M. and Bizzarro M. (2016) Chromatographic speciation of Cr(III)-species, inter-species equilibrium isotope fractionation and improved chemical purification strategies for high-precision isotope analysis. *J. Chromatogr. A* **1443**, 162–174.

Lauretta D. S., DellaGiustina D. N. and Bennett C. A., et al. (2019) The unexpected surface of asteroid (101955) Bennu. *Nature* **568**, 55–60.

Lee M. R., Lindgren P., Sofe M. R., Alexander C. M. O&rsquo and Wang J. (2012) Extended chronologies of aqueous alteration in the CM2 carbonaceous chondrites: evidence from carbonates in Queen Alexandria Range 93005. *Geochim. Cosmochim. Acta* **92**, 148–169.

Lee M. R., Lindgren P., King A. J., Greenwood R. C., Franchi I. A. and Sparkes R. (2016) Elephant Moraine 96029, a very mildly aqueously altered and heated CM carbonaceous chondrite: Implications for the drivers of parent body processing. *Geochim. Cosmochim. Acta* **187**, 237–259.

Lee M. R., Cohen B. E., King A. J. and Greenwood R. C. (2019) The diversity of CM carbonaceous chondrite parent bodies explored using Lewis Cliff 85311. *Geochim. Cosmochim. Acta* **264**, 224–244.

Martinez R. and Mason B. (1989) Description of sample MAC 88107. *Antarctic Meteorite Newslett.* **12**, 20.

Martins Z., Hoffmann B. A., Gnos E., Greenwood R. C., Verchovsky A., Franchi I. A., Jull A. J. T., Botta O., Glavin D. P., Dworkin J. P. and Ehrenfreund P. (2007) Amino acid composition, petrology, geochemistry, 14C terrestrial age and oxygen isotopes of the Shişr 033 CR chondrite. *Meteorit. Planet. Sci.* **42**, 1581–1595.

Mason B. (1987) Thin section description of LEW 85332,4. *Antarctic Meteorite Newslett.* **10**, 15.

Miller M. F., Franchi I. A., Sexton A. S. and Pillinger C. T. (1999) High precision $\Delta^{17}O$ isotope measurements of oxygen from silicates and other oxides: Methods and applications. *Rapid Comm. Mass Spec.* **13**, 1211–1217.

Nagashima K., Krot A. N. and Huss G. R. (2015) Oxygen-isotope compositions of chondrule phenocrysts and matrix grains in Kakangari K-grouplet chondrite: Implication to a chondrule-matrix genetic relationship. *Geochim. Cosmochim. Acta* **151**, 49–67.

Niederer F. R., Papanastassiou D. A. and Wasserburg G. J. (1981) The isotopic composition of titanium in the Allende and Leoville meteorites. *Geochim. Cosmochim. Acta* **45**, 1017–1031.

Olsen M. B., Wielandt D., Schiller M., Van Kooten E. M. M. E. and Bizzarro M. (2016) Magnesium and 54Cr isotope compositions of carbonaceous chondrite chondrules – Insights into early disk processes. *Geochim. Cosmochim. Acta* **191**, 118–138.

Piani L., Marrocchi Y., Rigaudier T., Vacher L. G., Thomassin D. and Marty B. (2020) Earth's water may have been inherited from material similar to enstatite chondrite meteorites. *Science (80-.)* **369**, 1110–1113.

Piralla M., Marrocchi Y., Verdier-Paoletti M. J., Vacher L. G., Villeneuve J., Piani L., Bekaert D. V. and Gounelle M. (2020) Primordial water and dust of the Solar System: Insights from in situ oxygen measurements of CI chondrites. *Geochim. Cosmochim. Acta* **269**, 451–464.

Qin L., Alexander C. M. O. D., Carlson R. W., Horan M. F. and Yokoyama T. (2010) Contributors to chromium isotope variation of meteorites. *Geochim. Cosmochim. Acta* **74**, 1122–1145.

Render J., Ebert S., Burkhardt C., Kleine T. and Brennecka G. A. (2019) Titanium isotopic evidence for a shared genetic heritage of refractory inclusions from different carbonaceous chondrites. *Geochim. Cosmochim. Acta* **254**, 40–53.

Righter K. (2007). *Antarctic Meteorite Newslett.* **30**, 1.

Rubin A. E. (1989) Size-frequency distributions of chondrules in CO3 chondrites. *Meteoritics* **24**, 179–189.

Rubin A. E. (2000) Petrologic, geochemical and experimental constraints on models of chondrule formation. *Earth Sci. Rev.* **50**, 3–27.

Rubin A. E. and Wasson J. T. (1986) Chondrules in the Murray CM2 meteorite and compositional differences between CM–CO and ordinary chondrite chondrules. *Geochim. Cosmochim. Acta* **50**, 307–315.

Rubin A. E. and Kallemeyn G. W. (1990) Lewis Cliff 85332: A unique carbonaceous chondrite. *Meteoritics* **25**, 215–225.

Rubin A. E. (2005) Relationships among intrinsic properties of ordinary chondrites: oxidation state, bulk chemistry, oxygen-isotopic composition, petrologic type, and chondrule size. *Geochim. Cosmochim. Acta* **69**, 4907–4918.

Russell S. S., McCoy T. J., Jarosewich E. and Ash R. D. (1998) The Burnwell, Kentucky, low-FeO chondrite fall: description, classification and origin. *Meteorit. Planet. Sci.* **33**, 853–856.

Russell S. S., Davis A. M., MacPherson G. J., Guan Y. and Huss G. R. (2000) Refractory inclusions from the ungrouped carbonaceous chondrites MAC 87300 and MAC 88107. *Meteorit. Planet. Sci.* **35**, 1051–1066.

Sanborn M. E., Wimpenny J., Williams C. D., Yamakawa A., Amelin Y., Irving A. J. and Yin Q. Z. (2019) Carbonaceous achondrites Northwest Africa 6704/6693: Milestones for early Solar System chronology and genealogy. *Geochim. Cosmochim. Acta* **245**, 577–596.

Satterwhite C. and Mason B. (1988) Description of MAC 87300. *Antarctic Meteorite Newslett.* **11**, 34.

Schiller M., Van Kooten E., Holst J. C., Olsen M. B. and Bizzarro M. (2014) Precise measurement of chromium isotopes by MC-ICPMS. *J. Anal. At. Spectrom.* **29**, 1406–1416.

Schneider J. M., Burkhardt C., Marrocchi Y., Brennecka G. A. and Kleine T. (2020) Early evolution of the solar accretion disk inferred from Cr-Ti-O isotopes in individual chondrules. *Earth Planet. Sci. Lett.* **551**, 116585.

Schrader D. L., Franchi I. A., Connolly, Jr., H. C., Greenwood R. C., Lauretta D. S. and Gibson J. M. (2011) The formation and alteration of the Renazzo-like carbonaceous chondrites I: Implications of bulk-oxygen isotopic composition. *Geochim. Cosmochim. Acta* **75**, 308–325.

Schrader D. L., Davidson J., Greenwood R. C., Franchi I. A. and Gibson J. M. (2014) A water-ice rich minor body from the early Solar System: The CR chondrite parent asteroid. *Earth Planet. Sci. Lett.* **407**, 48–60.

Schrader D. L. and Davidson J. (2017) CM and CO chondrites: A common parent body or asteroidal neighbors? Insights from chondrule silicates. *Geochim. Cosmochim. Acta* **214**, 157–171.

Schrader D. L., McCoy T. J. and Gardner-Vandy K. (2017a) Relict chondrules in primitive achondrites: Remnants from their precursor parent bodies. *Geochim. Cosmochim. Acta* **205**, 295–312.

Schrader D. L., Nagashima K., Krot A. N., Ogliore R. C., Yin Q.-Z., Amelin Y. A., Stirling C. H. and Kaltenbach A. (2017b) Distribution of ^{26}Al in the CR chondrite chondrule-forming region of the protoplanetary disk. *Geochim. Cosmochim. Acta.* **201**, 275–302.

Scott E. R. D. and Krot A. N. (2014) Chondrites and their components. In *Treatise on Geochemistry* (eds. H. D. Holland and K. K. Turekian), vol. 1, second ed. Elsevier, Oxford, pp. 65–137.

Shields W. R., Murphy J. T., Cantazaro E. J. and Garner E. L. (1966) Absolute isotopic abundance ratios and the atomic weight of a reference sample of chromium. *J. Res. Natl. Bur. Stand.* **70A**, 193–197.

Shukolyukov A. and Lugmair G. W. (2006) Manganese-chromium isotope systematics of carbonaceous chondrites. *Earth Planet. Sci. Lett.* **250**, 200–213.

Starkey N. A., Jackson C. R. M., Greenwood R. C., Parman S., Franchi I. A., Jackson M., Fitton J. G., Stuart F. M., Kurz M. and Larsen L. M. (2016) Triple oxygen isotopic composition of the high $^{3}He/^{4}He$ mantle. *Geochim. Cosmochim. Acta* **176**, 227–238.

Sugiura N. and Fujiya W. (2014) Correlated accretion ages and $\varepsilon^{54}Cr$ of meteorite parent bodies and the evolution of the solar nebula. *Meteorit. Planet. Sci.* **49**, 772–787.

Torrano Z. A., Brennecka G. A., Williams C. D., Romaniello S. J., Rai V. K., Hines R. R. and Wadhwa M. (2019) Titanium isotope signatures of calcium-aluminum-rich inclusions from CV and CK chondrites: Implications for early Solar System reservoirs and mixing. *Geochim. Cosmochim. Acta* **263**, 13–30.

Trinquier A., Birck J.-L. and Allègre C. J. (2007) Widespread ^{54}Cr heterogeneity in the inner solar system. *Astrophys. J.* **655**, 1179–1185.

Trinquier A., Elliott T., Ulfbeck D., Coath C., Krot A. N. and Bizzarro M. (2009) Origin of nucleosynthetic isotope heterogeneity in the solar protoplanetary disk. *Science* **324**, 374–376.

Troiano J., Rumble, III, D., River M. L. and Friedrich J. M. (2011) Compositions of three low-FeO ordinary chondrites: Indications of a common origin with the H chondrites. *Geochim. Cosmochim. Acta* **75**, 6511–6519.

Warren P. H. (2011) Stable-isotopic anomalies and the accretionary assemblage of the Earth and Mars: A subordinate role for carbonaceous chondrites. *Earth Planet. Sci. Lett.* **311**, 93–100.

Wasson J. T., Rubin A. E. and Kallemeyn G. W. (1993) Reduction during metamorphism of four ordinary chondrites. *Geochim. Cosmochim. Acta* **57**, 1867–1878.

Weisberg M. K., Prinz M., Clayton R. N. and Mayeda T. K. (1993) The CR (Renazzo-type) carbonaceous chondrite group and its implications. *Geochim. Cosmochim. Acta* **57**, 1567–1586.

Weisberg M. K., McCoy T. J. and Krot A. N. (2006) Systematics and evaluation of meteorite classification. In *Meteorites and the Early Solar System II* (eds. D. S. Lauretta and H. Y. McSween). University of Arizona Press, Tucson, pp. 19–52.

Williams C. D., Sanborn M. E., Defouilloy C., Yin Q.-Z., Kita N. T., Ebel D. S., Yamakawa A. and Yamashita K. (2020) Chondrules reveal large-scale outward transport of inner Solar System materials in the protoplanetary disk. *Proc. Natl. Acad. Sci.*, 23426–23435.

Yamaguchi A., Kimura M., Barrat J.-A. and Greenwood R. (2019) Compositional diversity of ordinary chondrites inferred from petrology, bulk chemical, and oxygen isotopic compositions of the lowest FeO ordinary chondrite, Yamato 982717. *Meteorit. Planet. Sci.* **54**, 1919–1929.

Yamakawa A., Yamashita K., Makishima A. and Nakamura E. (2009) Chemical Separation and Mass Spectrometry of Cr, Fe, Ni, Zn, and Cu in Terrestrial and Extraterrestrial Materials Using Thermal Ionization Mass Spectrometry. *Anal. Chem* **81**, 9787–9794.

Yamakawa A., Yamashita K., Makishima A. and Nakamura E. (2010) Chromium Isotope Systematics of Achondrites: Chronology and Isotopic Heterogeneity of the Inner Solar System Bodies. *Astrophys. J.* **720**, 150–154.

Yamashita K., Maruyama S., Yamakawa A. and Nakamura E. (2010) ^{53}Mn–^{53}Cr chronometry of CB chondrite: Evidence for uniform distribution of ^{53}Mn in the early Solar System. *Astrophys. J.* **723**, 20–24.

Zhang J., Dauphas N., Davis A. M. and Pourmand A. (2011) A new method for MC-ICPMS measurement of titanium isotopic composition: Identification of correlated isotope anomalies in meteorites. *J. Anal. At. Spectrom.* **26**, 2197–2205.

Zhang J., Dauphas N., Davis A. M., Leya I. and Fedkin A. (2012) The proto-Earth as a significant source of lunar material. *Nature Geosci.* **5**, 251–255.

Zolensky M., Barrett R. and Browning L. (1993) Mineralogy and composition of matrix and chondrule rims in carbonaceous chondrites. *Geochim. Cosmochim. Acta* **57**, 3123–3148.

Associate editor: Thorsten Kleine